A genetic screen identifies a protective type III interferon response to *Cryptosporidium* that requires TLR3 dependent recognition

Alexis R. Gibson[1], Adam Sateriale[1,2], Jennifer E. Dumaine[1], Julie B. Engiles[1,3], Jodi A. Gullicksrud[1], Keenan O'Dea[1], John G. Doench[4], Daniel P. Beiting[1], Christopher A. Hunter[1], Boris Striepen[1]†

[1]Department of Pathobiology, School of Veterinary Medicine, University of Pennsylvania, Philadelphia, PA, 19104

[2]Current: The Francis Crick Institute, London NW1 1AT, United Kingdom.

[3]Department of Pathobiology, New Bolton Center, School of Veterinary Medicine, University of Pennsylvania, Philadelphia, PA 19348, United States of America.

[4]Genetic Perturbation Platform, Broad Institute of MIT and Harvard, Cambridge, MA, USA.

†To whom correspondence should be addressed: Tel.: 1-215-573-9167; Fax: 1-215-746-2295; email: striepen@upenn.edu

Short title: *Cryptosporidium,* IFN-lambda, and TLR3

Abstract

Cryptosporidium is a leading cause of severe diarrhea and diarrheal-related death in children worldwide. As an obligate intracellular parasite, *Cryptosporidium* relies on intestinal epithelial cells to provide a niche for its growth and survival, but little is known about the contributions that the infected cell makes to this relationship. Here we conducted a genome wide CRISPR/Cas9 knockout screen to discover host genes required for *Cryptosporidium parvum* infection and/or host cell survival. Gene enrichment analysis indicated that the host interferon response, glycosaminoglycan (GAG) and glycosylphosphatidylinositol (GPI) anchor biosynthesis are important determinants of susceptibility to *C. parvum* infection. Several of these pathways are linked to parasite attachment and invasion and C-type lectins on the surface of the parasite. Evaluation of transcript and protein induction of innate interferons revealed a pronounced type III interferon response to *Cryptosporidium* in human cells as well as in mice. Treatment of mice with IFNλ reduced infection burden and protected immunocompromised mice from severe outcomes including death, with effects that required STAT1 signaling in the enterocyte. Initiation of this type III interferon response was dependent on sustained intracellular growth and mediated by the pattern recognition receptor TLR3. We conclude that host cell intrinsic recognition of *Cryptosporidium* results in IFNλ production critical to early protection against this infection.

Author Summary

Cryptosporidium infection is an important contributor to global childhood mortality. There are currently no vaccines available, and the only drug has limited efficacy in immunocompromised individuals and malnourished children who need it most. To discover which host proteins are essential for *Cryptosporidium* infection, we conducted a genome wide knockout screen in human host cells. Our results confirm the importance of glycosaminoglycans on the surface of epithelial cells for attachment and invasion of the parasite. We also found that host GPI anchor biosynthesis and interferon signaling pathways were enriched by our screen. Examining the role of interferon signaling further we found a type III interferon response, IFNλ, was generated in response to infection and shown to be initiated in the infected cell. Utilizing mouse models of infection, we found that the type III interferon response was important early during infection with its induction likely preceding IFNγ, a key cytokine for the control of this infection. We also determined that TLR3 was the pattern recognition receptor responsible for IFNλ production during *Cryptosporidium* infection. Our work shows that IFNλ acts directly on the enterocyte and its use in treating immunocompromised mice produced striking reductions in infection.

Introduction

Cryptosporidium is a leading cause of diarrheal disease. In the United States, this apicomplexan parasite accounts for more than half of all waterborne disease outbreaks and infection can be life-threatening in individuals with compromised immune function [1, 2]. Globally, the burden of this disease rests disproportionally on children under the age of two and the parasite is an important contributor to early childhood mortality [3]. Children can experience multiple episodes of infection, however, parasite and disease burden diminish over successive infection and non-sterile immunity protects children from severe illness as well as stunting [4].

It is well established that T cells are critical to protection from and the resolution of infection with *Cryptosporidium* [5]. The production of interferon gamma (IFNγ) is recognized to be one of the essential functions of T cells during *Cryptosporidium* infection [6], but T cells are not the only source of IFNγ [7-9]. Numerous other chemokines and cytokines produced by the enterocyte including IL-8, IL-18, TGFβ, and RANTES and type one and three interferons have been noted as well [10-14]. These can act directly on enterocytes and/or stimulate responses by proximal immune cells in the intestinal epithelium and adjacent tissues leading to the enhanced production of IFNγ, among other responses. IL-18 was shown to be produced by the enterocyte and to signal to ILC1s promoting IFNγ production [9]. New *in vitro* enteroid models of infection have also revealed the presence of a type I IFN response through RNA sequencing [15, 16]. Additionally, type III interferon (IFNλ) production has been observed in response to *C. parvum* infection in neonatal piglets and neonatal mice [12]. Type III interferons, the most recently discovered members of the cytokine family, were shown to play unique roles at

mucosal sites that could not be compensated for by type I interferons [17] making their role during *Cryptosporidium* infection of particular interest..

Cryptosporidium infection is typically restricted to the small intestine, but infection of the biliary tree and respiratory involvement has also been reported [18, 19]. Within the intestine, the infection is limited to epithelial cells in which the parasite occupies an intracellular but extra-cytoplasmic niche at the brush border. A number of cytoskeletal and membranous structures separate the parasitophorous vacuole from the bulk of the infected enterocyte [20, 21]. While reorganization of the actin cytoskeleton is one of the most prominent changes in host cell morphology, infection is also known to interfere with the composition and function of tight junctions, to induce tyrosine phosphorylation, and to activate PI3K signaling [22, 23]. Recent studies have identified parasite proteins that are injected into the host cell during and after invasion [24, 25] but we know very little about the specific components of the host cell that shape host-parasite interaction for *Cryptosporidium*.

Here, we used a CRISPR-Cas9 knockout screen to identify host genes that impact host cell survival during *Cryptosporidium* infection. The screen revealed the importance of several pathways, with IFN signaling, sulfated GAGs, and GPI anchor synthesis most prominent. We found that the interferon signaling pathway identified here was triggered by robust production of type III but not type I interferon in human host cells. This response required live infection and was initiated in infected cells. We investigated the molecular recognition mechanism that leads to this response and studied its impact on the infection. *In vivo* experiments showed IFNλ to limit parasite growth an effect that was independent

of the presence of IFNγ. Thus, we elucidate a mechanism of cell intrinsic recognition and control of *Cryptosporidium*.

Results

A screen for host genes that impact *Cryptosporidium* infection and host cell survival

How *Cryptosporidium* interacts with its host cell is poorly understood. The parasite is thought to rely on pathogenesis factors exposed on its surface or secreted during and after invasion [26, 27], however, host proteins are likely to play important roles in this interaction as well. To identify such host factors, we conducted an unbiased genetic screen. Since *Cryptosporidium* infection is limited to epithelial cells, we chose to screen in HCT-8 cells, a colon-derived human adenocarcinoma cell line widely used for experiments with this parasite [28]. In this *in vitro* culture system, parasites can only be propagated for 72 hours and then growth ceases. First, we measured the survival of HCT-8 cells over a range of infection conditions and found *C. parvum* to induce host cell death in a dose-dependent fashion over the 72 hours (Fig 1A). We chose to move forward with a 90% kill dose to impose strong selection for loss of function in genes required for parasite growth or cell death as part of the host response to infection. Next, we generated clonal HCT-8 cell lines that stably express Cas9 [29] and assessed activity in each clone using an EGFP reporter assay [30]. Briefly, Cas9 expressing cells were transfected with a lentiviral vector encoding EGFP as well as a single guide RNA (sgRNA) targeting the EGFP gene and analyzed by flow cytometry. Cells with Cas9 activity show reduced fluorescence when compared to the parental cell line and are shown normalized to a

control cell line expressing no EGFP (Fig 1B). Clones C, I, and K showed high activity and served as three independent biological replicates in the subsequent screen. Using the Brunello lentiviral CRISPR library, we targeted the full complement of human protein coding genes with four sgRNAs each in addition to controls [31] for a total of 77,441 sgRNAs. 10^8 cells of each clone were transduced with the library at an MOI of 0.4 to ensure each cell received only one sgRNA. Following seven days of puromycin selection, cells were expanded to 4 T175 flasks, achieving roughly 500-fold coverage and infected with *C. parvum* at a 90% kill dose. After 72 hours, the media was changed, and surviving cells were allowed to expand. Cells were exposed to *C. parvum* for a total of three rounds of infection and expansion to enrich for resistant host cells (Fig 1C). Genomic DNA was extracted from the input population as well as following each round of infection.

Genetic screen reveals genes required for infection and host response

Deep sequencing of the integrated sgRNAs and comparison with the input population revealed the progressive enrichment of a subset of sgRNAs with each round of infection (Fig 1D). Using model-based analysis of genome-wide CRISPR/Cas9 knockout [32], we identified 35 significantly enriched genes (FDR < 0.05, Fig 1E). Among these genes, gene set enrichment analysis (GSEA) reveals three distinct pathways each supported by multiple genes. IFNAR2, IFNLR1, IL10RB, IRF9, STAT1, STAT2, JAK1, and TYK2 cluster within the pathway of interferon (IFN) signaling. B3GAT3, B4GALT7, EXT1, SLC35B2 are genes encoding enzymes in the biosynthesis of sulfated glycosaminoglycans (GAG). In addition, the screen selected for nine enzymes required for glycosylphosphatidylinositol (GPI) anchor biosynthesis (GPAA1, MGAT1, PGAP2, PIGA, PIH, PIGL, PIGO, PIGP, PIGT). Beyond these pathways, a number of genes were

150 significantly enriched that were not members of a particular pathway or represented the
151 single representative of a pathway. Among those with known molecular function were
152 accessory proteins to ATP flippase (TMEM30A), tyrosine protein kinases (CSK), GTPase
153 activators (RALGAPB), G protein coupled receptor signaling regulators (PDCL), granule
154 biogenesis proteins (NBEAL2), transcriptional activators of apoptosis (RRP1B),
155 dehalogenases (IYD), tetraspanins (CD151), fibronectin domain proteins (FNDC3B),
156 chaperones (UNC93B1 and HSP90B1), transcription factors (OLIG1), serine protease
157 (TMPRSS3), and peptide hormone receptors (NPR3).

158 To validate the screening results, HCT-8 cells were transduced with siRNA
159 targeting a subset of the top candidates for 24 hours prior to infection. Knockdown was
160 assessed by qPCR and a decrease in transcripts was found to be typically 30% or greater.
161 48 hours after *C. parvum* infection, we assessed host cell viability using the MTT assay.
162 We found that many candidates when knocked down, show increased resistance to cell
163 death, no difference was noted in the absence of infection (S1 Fig).

164

165 **_Cryptosporidium parvum_ infection induces an interferon response**

166 Interferon signaling was the most highly enriched pathway identified by our screen.
167 The critical role of IFNγ is well documented in humans [33] and mice [5] and there are
168 also reports of *Cryptosporidium* associated induction of type I and III interferons [12, 13,
169 15]. To examine the epithelial cell response to *C. parvum*, we infected 6 well cultures of
170 HCT-8 cells with 100,000 oocysts and performed RNAseq. 1600 genes were differentially
171 expressed (1.5-fold; adjusted p value < 0.05) by 48 hours post infection, compared to
172 naïve cells (Fig 2A). The majority of differentially expressed genes were upregulated in

the infected population compared to the uninfected control (689 genes downregulated). GSEA identified significant enrichment of the interferon signaling pathway in infected cultures compared to uninfected controls (Fig 2B). Other strongly enriched pathways are related to interferon signaling, such as REACTOME: Antiviral Mechanism by IFN Stimulated Genes.

To validate the observed interferon signature and to establish kinetics, we next conducted a qPCR time course experiment for three selected interferon stimulated genes (ISGs) over 72hours of *C. parvum* infection to determine when the interferon response is initiated. We infected 96-well cultures with *C. parvum* and isolated RNA at 0, 12, 24, 48, and 72 hours post infection. ISG transcripts were increased in the first sample taken at 12 hours post infection and peaked at 72 hours (Fig 2C). Binding of interferons to their receptors initiates an intracellular signaling cascade that culminates in the phosphorylation of the transcription factor STAT1 leading to transcription of ISGs. We therefore assessed STAT1 phosphorylation by Western Blot using a modification specific antibody in whole cell lysates. Phosphorylation of STAT1 was not detectable in uninfected cells but was observed as early as 12 hours post infection (Fig 2D). We also observed an increase in total STAT1 protein at 24 hours post infection indicating that STAT1 itself was induced by the infection, in line with its classification as an ISG. We conclude that *C. parvum* infection induces a strong interferon response in HCT-8 cells.

Cryptosporidium **infection preferentially induces a type III interferon response**

Next, we asked which interferon was responsible for the response observed. There are three major interferon types; type II interferon, IFNγ, is only produced by certain

196 lymphocytes and thus absent from our cultures. In contrast, type I interferons, most
197 prominently IFNα and IFNβ, and type III interferons, IFNλ 1-4, are known to be produced
198 by epithelial lineages including the HCT-8 cells used here [34] (S2 Fig). Our GSEA
199 analyses found enrichment signatures for type I and type III interferon in infected cultures
200 (S2 Fig), but because both types act through the same intracellular signaling cascade, it
201 is difficult to distinguish between them by the genes they induce [35]. To determine which
202 types of interferons are expressed - simultaneously or individually - in response to *C.*
203 *parvum*, we measured the transcript abundance of *IFNB*, *IFNL1*, and *IFNL2/3* by qPCR.
204 *IFNB* transcripts did not increase at early time points and remained comparably low at 72
205 hours (4-fold, Fig 2E). In contrast, at 12 hours, the first time point sampled, type III
206 interferon transcripts were already markedly elevated. Type III interferon transcripts
207 peaked at 48 hours (*IFNL1*: 35-fold, *IFNL2/3*:1200-fold). We also performed enzyme-
208 linked immunosorbent assays (ELISA) to directly measure protein levels
209 for IFNβ and IFNλ. Only modest amounts of IFNβ were detectable, peaking at 48 hours
210 post infection (185 pg/mL). IFNλ production was detected as early as 24 hours post
211 infection and continued to increase until 72 hours, exceeding IFNβ levels by two orders
212 of magnitude (16,029 pg/mL, p <0.0001, Two-way ANOVA, Fig 2F). The kinetics of the
213 induction of IFNλ protein followed that of parasite replication, with a large increase
214 between 24 and 48 hours, when the parasites were actively replicating, and a plateau
215 between 48 and 72 hours when parasites terminally differentiate to gametes and growth
216 ceases (Fig 2G and [36]). Taken together, these experiments demonstrate that type III,
217 rather than type I interferons are preferentially induced by *C. parvum* infection in HCT-8
218 cells.
219

Live *C. parvum* infection is required to induce type III interferon production

A variety of pathogen associated molecular patterns (PAMPs) have been shown to induce a type III interferon response including many bacterial proteins, glycans and lipids [37]. Oocysts used in our experiments were isolated from the feces of cows or mice; therefore, we considered that inadvertent inoculation of cultures with bacterial PAMPS rather than *C. parvum* infection may drive IFNλ production. To test this, we heated oocysts to 95°C for 10 min prior to adding them to cells. This kills the parasite but does not inactivate LPS [38]. Heat killed parasites failed to induce IFNλ at any timepoint assessed, and at 72 hours post infection, the difference in IFNλ production compared to controls was highly significant (Fig 3A, $p < 0.0001$, Two-way ANOVA). Consistent with the lack of IFNλ production, we did not observe phosphorylation of STAT1 in cultures inoculated with heat killed parasites (Fig 3B). To further assess the importance of parasite replication for interferon induction, we used nitazoxanide, the only currently FDA approved drug for the treatment of *Cryptosporidium* infection. Treatment of cultures led to a 35-fold decrease in parasite infection as assessed by qPCR (Fig 3C). In the nitazoxanide treated infected cultures, IFNλ induction was no longer observed (Fig 3D, $p < 0.05$, One-way ANOVA). In contrast, the induction of IFNλ using an agonist of interferon signaling, Poly(I:C), was intact under nitazoxanide treatment, demonstrating that the observed response is specific to parasite infection. We therefore conclude that live parasites and active parasite replication are required to induce the type III interferon response.

IFN-lambda is initially produced by infected cells and signals in an autocrine manner

The parasite completes its replicative cycle within 12 hours and parasite egress is accompanied by host cell lysis and the release of intracellular contents, including both host and parasite molecules (Fig 3E). Both intracellular parasite growth, and/or host cell lysis could trigger the interferon response. Furthermore, signaling, once initiated, results in the secretion of interferons, which may act on both producing and surrounding cells in an auto- as well as paracrine fashion. This amplifies the signal through a feedforward loop rapidly leading to cytokine from essentially all cells, making it difficult to determine how the cascade originates.

To determine the cells that initiate the type III interferon response, we infected HCT-8 with a *C. parvum* strain marked by expression of tandem Neon green fluorescent protein (Fig 3F). At 10 hours post infection, and prior to first parasite egress, we sorted cells for green fluorescence and isolated Neon positive infected cells as well as Neon negative bystander cells from the same culture (Fig 3G). Three biologically independent samples were subjected to RNA sequencing for each population. Infection resulted in significant differences in gene expression with 380 upregulated and 466 downregulated genes (1.5-fold; adjusted p value < 0.05, Fig 3H). We noted the induction of IFNL1 and 126 additional ISGs as identified by Interferome DB [39]. Many of these genes represent a subset of the interferon signature we observed in our 48-hour RNAseq but the amplitude of expression was lower, likely a reflection of the early timepoint and the lack of paracrine amplification. Importantly, at this timepoint induction of the interferon pathway is exclusive to infected Neon positive cells. We conclude that the type III interferon response is initiated during intracellular replication of *C. parvum* in a cell intrinsic fashion.

The type III interferon response is required for early in vivo host defense

To understand the consequences of the type III interferon response on infection, we turned to an *in vivo* model of infection that uses a *C. parvum* strain adapted to mice by continued serial passage [9]. First, we asked whether and when type III interferons are produced in response to *C. parvum in vivo.* At day 2 post infection of C57BL/6 mice, we found an average 4-fold increase of *Ifnl2/3* transcripts in the small intestine, and at day 4, the induction was approximately 2-fold. (Fig 4A). We also assessed IFNλ secretion during *C. parvum* infection using an ELISA from punch biopsies of the ileum and found similar kinetics. IFNλ secretion was increased at 2 days post infection and waned below detectable levels after 4 days (Fig 4B).

Type I and III interferons initiate a similar intracellular signaling cascade but utilize different receptors, IFNAR for type I and a heterodimer of IFNLR1 and IL10RB for type III. We infected C57BL/6 wild type mice, mice lacking the type I interferon receptor, Ifnar$^{-/-}$, and mice lacking the type III interferon receptor, Il28ra$^{-/-}$, with 50,000 *C. parvum* oocysts. Infection was monitored by measuring parasite produced Nanoluciferase from feces [40]. Surprisingly, loss of the type I interferon receptor consistently resulted in a 3-fold reduction in shedding when compared to wild type mice (area under the curve (AUC), Fig 4C). In contrast, loss of type III interferon signaling resulted in an overall 2.7-fold increase in parasite shedding compared to wild type mice (AUC, Fig 4C). We note that histopathology revealed no baseline differences between WT and Il28ra$^{-/-}$ mice (S3 Fig). To further validate this finding independent of mouse mutants, we used antibody-based depletion. C57BL/6 mice were intraperitoneally injected daily with 20μg of an anti-Ifnλ2/3 antibody and infected with 50,000 *C. parvum* oocysts. Again, we observed an increase in

parasite shedding of about 2-fold (AUC, Fig 4D). We conclude that type III, but not type I interferons contribute to the early control of *Cryptosporidium in vivo*.

Exogenous IFN-lambda treatment protects mice from severe *Cryptosporidium* infection

Since mice lacking the type III interferon receptor exhibited an increase in early susceptibility, we tested the impact of exogenous administration of IFNλ on *Cryptosporidium* infection. Ifng$^{-/-}$ mice were injected intraperitoneally with daily doses of Ifnλ2 ranging from 0-5μg for the first three days of infection. As little as 0.1μg per day (the smallest amount tested) produced a marked reduction in shedding (4.3-fold decrease AUC, Fig 4E), and increasing the dose beyond 1μg did not yield further enhancement. To assess whether this effect could be maintained long term, Ifng$^{-/-}$ mice were infected with *C. parvum* and injected intraperitoneally with a daily dose of 1μg Ifnλ2 for the duration of the infection. This treatment resulted in 7.7-fold reduction of shedding when compared to mock injected control infections (AUC, Fig 4F). In contrast to mock injected mice, we did not observe mortality among treated mice.

We note that administration of IFNλ was protective in Ifng$^{-/-}$ mice, suggesting that this protection does not require IFNγ. However, IFNλ has been shown to promote IFNγ production [41]. To examine this potential interaction further we tested the effect of IFNλ in mice lacking cells known to produce IFNγ in response to *C. parvum*: T cells, NK cells and ILCs [7, 9, 42]. BL6, Rag2$^{-/-}$, and Rag2$^{-/-}$Il2rg$^{-/-}$ mice were infected and treated with 1μg of Ifnλ2. This resulted in comparable reduction of parasite shedding (BL6: 2.4-fold, Rag2$^{-/-}$: 4.4-fold, Rag2$^{-/-}$Il2rg$^{-/-}$: 2-fold, Fig 4G), again suggesting that the benefit of IFNλ

313 treatment does not require immune cells, but largely rests on an enterocyte intrinsic
314 response. Finally, we conducted experiments with mice in which the STAT1 gene was
315 specifically ablated from enterocytes using Cre recombinase under the control of the
316 *Villin1* promoter. Removing STAT1 from the enterocyte lineage alone abolished the
317 benefit of IFNλ treatment (1.1-fold AUC, Fig 4H). Taken together, these data suggest that
318 IFNλ protects mice and does so by acting directly on the intestinal epithelium.
319
320 **TLR3 detects *Cryptosporidium* infection leading to IFN-lambda production**
321 Enterocytes have been shown to use a range of pattern recognition receptors to
322 detect infection with different pathogens, many of which can lead to a type III interferon
323 response [43]. HCT-8 cells, as many other cancer-derived lines, no longer express the
324 full complement of innate immune recognition and cell death pathways [44], but the IFNλ
325 response to *Cryptosporidium* remains intact. We took advantage of this to narrow the list
326 of potential receptors. HCT-8 cells were treated with known agonists of different pattern
327 recognition receptors and IFNλ production was measured after 24 hours. Specifically, we
328 tested Poly(I:C) with or without lipofection (TLR3 and RLRs), mTriDAP (NOD1 and
329 NOD2), 5' triphosphate dsRNA (RIGI), HSV60 DNA (CDS), ssPolyU RNA (TLR7), or CpG
330 motif containing DNA (TLR9) [45]. As shown in Fig 5A, only Poly(I:C) and ssPolyU RNA
331 produced an IFNλ response. This suggests TLR3, TLR7, or the RLRs MDA5 and RIGI as
332 potential receptors. We next tested each of these candidates *in vivo* using suitable mouse
333 mutants. Mice lacking MAVS, the adapter protein to RLRs, and TLR7 showed no
334 difference in infection compared to wild type controls (Fig 5B and 5C). However, mice
335 lacking TLR3 were more susceptible, resulting in an 8-fold increase in parasite shedding

and an overall pattern of infection that was reminiscent of Il28ra$^{-/-}$ mice (AUC, Fig 5D). We found the production of IL-18, an enterocyte derived cytokine induced by *Cryptosporidium* infection, [46, 47] to be intact in the absence of TLR3 (Fig 5E). Next, we measured IFNλ secretion from ileal punches of infected Tlr3$^{-/-}$ mice and wild type controls at day 2 of infection by ELISA. In the absence of TLR3, IFNλ production was reduced to the limit of detection (Fig 5F, *p* value < 0.001, Unpaired t-test). Note this reduction occurs despite an 8-fold higher infection in Tlr3$^{-/-}$. We conclude that the production of type III IFN during *Cryptosporidium* infection depends on TLR3 signaling.

Discussion

We conducted a whole genome knock out screen to identify human genes that influence *Cryptosporidium* infection and host survival. We identified 35 genes with high confidence, and they implicate multiple pathways.

Parasite attachment and invasion

Four of the genes enriched in our screen encode steps in the synthesis of glycosaminoglycans. This provides further support for the notion that interactions between a parasite C-type lectin and host glycosaminoglycans are critical to parasite binding and invasion [48]. GPI anchor synthesis is also highly prominent among the enriched genes. GPI anchored proteins are preferentially targeted to the apical membrane of polarized cells [49], the membrane used by the parasite to invade. GPI anchored proteins are thus exposed to the parasite. Among them are glypicans which serve as the platform of apically displayed membrane associated glycosaminoglycans in the intestine [50]. The screen also identified the tetraspanin CD151. Interestingly, in infected cells this host protein is recruited to the host-parasite interface (S4 Fig). CD151 is critical to the uptake and intracellular trafficking of human cytomegalovirus and pappilomavirus [51], and the related protein CD81 is required for the invasion of hepatocytes by *Plasmodium* sporozoites [52]. Tetraspanins act as scaffolds forming membrane microdomains that mediate adhesion, signaling, fusion and fission, and CD151 is well known for its role in integrin signaling [53]. Candidate FNDC3B contains a fibronectin type III domain involved in interactions with integrins and knockdown of this genes in HCT8 leads to a decrease in phosphorylation of PI3K [54]. Polymerization of

host actin is a prominent feature of *Cryptosporidium* invasion and host modification and there is evidence for parasite engagement of host integrins and PI3K signaling [55, 56] in this context.

Cellular signaling and membrane trafficking

The screen also identified the kinase CSK, a negative regulator of Src family kinases. c-Src kinase was shown to play an important role in host actin polymerization during *Cryptosporidium* infection [23]. Traditionally, this has been viewed as aiding parasite infection; however, recent studies may suggest a more complex picture in which the cortical cytoskeleton might also act in host defense [24, 57]. Src family kinases are also critical to pattern recognition receptor mediated detection of pathogens leading to the production of interferons and CSK is critical to tune this response [58, 59].

Multiple hits may impact membranes and their trafficking including NBEAL2, TMEM30A, and RALGAPB. RALGAPB is an inhibitor of the small GTPases RalA and RalB, which in turn activates the exocyst complex. In epithelial cells the exocyst is critical to exocytosis as well as the dynamic remodeling of the actin cytoskeleton [60]. RalA activity is required for membrane recruitment to the *Salmonella typhimurium* infection site [61]. TMEM30A is an essential binding partner of P4 type ATPase flippases and directs the trafficking of the catalytic subunits from the trans-Golgi to the plasma membrane [62]. Deletion of TMEM30A leads to defects in both endocytosis and exocytosis due to a loss of the asymmetric distribution of phospholipids across the plasma membrane [63]. NBEAL2 is required for the formation of secretory granules in a variety of cells [64]. At least two hits act on nucleotide signaling, PDCL or phosducin-like G-protein, is a chaperone of G-

protein beta gamma dimers [65] and erythrocyte G-proteins have been shown to play a role in *Plasmodium falciparum* invasion [66]. NPR3 is a G-protein coupled receptor which binds polypeptide hormones termed natriuretic peptides. Binding to this receptor inhibits adenylate cyclase and decreases cAMP [67].

Innate immunity

By far the most prominent pathway to emerge from our screen was interferon signaling. As we demonstrate in this study, *Cryptosporidium* infection leads to the production and rapid accumulation of high levels of IFNλ in HCT-8 cultures. The screen selected for host cell growth and survival, and interferons are potent inducers of cell death programs [68, 69]. Interferons can arrest the cell cycle of target cells and induce apoptosis, necroptosis, and autophagy [70-73].

The role of IFNγ in cryptosporidiosis is well established, but there have also been reports of interferons directly produced by the enterocyte during *Cryptosporidium* infection. Barakat et al., described the production of type I interferons in response to *C. parvum* infection in a mouse cell line [13]. Transcriptional profiling of infected organoids from the lung and small intestine revealed a signature that was similarly interpreted as response to type I IFN signaling [15, 16]. In contrast, Ferguson et al. recently reported type III interferon production in response to *C. parvum* infection in neonatal piglets and neonatal mice [12]. Their studies further suggest that IFNλ may block parasite invasion and promote barrier integrity during *C. parvum* infection.

In this study we show pronounced production of type III, but not type I interferons in human cells (Fig 6). We found the response to be initiated intrinsically in the infected

cell (Fig 3H) and amplified by an autocrine loop. Experiments *in vivo* demonstrated a protective role for IFNλ that did not require IFNγ or adaptive immunity but relied exclusively on signaling in enterocytes (Fig 4G, Fig 5H). Further, we discovered the pattern recognition receptor, TLR3, to be required for type III interferon production. TLR3 recognizes dsRNA, and we used the synthetic analog Poly (I:C) to induce IFNλ production. Previous studies have shown that injection of Poly (I:C) reduced *C. parvum* infection [74].

TLR3 is known to recognize other protozoan parasites including Neospora [75] and *Leishmania* [76] where it induces type I IFN production. For *Leishmania*, TLR3 recognition was dependent on the presence of a dsRNA virus found in certain parasite isolates. Interestingly, *Cryptosporidium* is also host to a dsRNA viral symbiont which could be a possible source of dsRNA recognized by TLR3 [77, 78]. In contrast to leishmaniasis where type I IFN production exacerbates disease [79], the type III interferon response to *C. parvum* is host protective. There have also been reports of *Cryptosporidium* derived RNAs to be trafficked into the host cell nucleus during infection providing an additional potential trigger for TLR3 [80]. While our screen did not identify TLR3 as a top candidate, UNC93B1, a protein critical to proper trafficking of endosomal TLRs [81], was a highly enriched gene. Cryptosporidiosis is most dangerous in children below the age of two years and it is thus noteworthy that TL3 is poorly expressed in neonates, and that low levels of TLR3 in the intestinal epithelium have been linked to the heightened susceptibility of neonatal mice to rotavirus [82].

The increase in parasite burden in mice lacking TLR3 exceeded that of mice lacking IFNLR1 (8-fold compared to 2.5-fold), potentially pointing towards TLR3 functions

436 beyond induction of type III interferon in epithelial cells. TLR3 is known to promote cross-
437 priming of CD8+ T cells via DC phagocytosis of virus infected cells [83]. The absence of
438 TLR3 signaling can impair the production of IL-12 by DCs [84] which is important for the
439 control of *Cryptosporidium* infection [85].

440 We recently reported that an enterocyte intrinsic NLRP6 inflammasome is
441 activated by *Cryptosporidium* infection leading to release of IL-18 [14]. This IL-18 in
442 conjunction with IL-12 then promotes downstream IFNγ production by ILCs [9]. Here we
443 describe a second parasite detection mechanism that depends on TLR3 and produces a
444 rapid IFNλ response that precedes the production of IFNγ by NK/ILCs and T cells. IFNλ
445 has been shown to augment the IFNγ response of NK cells via a mechanism involving IL-
446 12 [41]. Consistent with this idea treatment of $Rag2^{-/-}Il2rg^{-/-}$ was repeatedly less effective
447 than that of $Rag2^{-/-}$ alone (Fig 4G), suggesting a potential role for IFNλ in promoting IFNγ
448 production in NK/ILCs. However, loss of STAT1 exclusively in the enterocyte lineage led
449 to almost a complete abrogation of the effects of IFNλ treatment (Fig 4H), arguing that
450 the primary role of IFNλ is to act on the enterocyte. The protective effects of IFNλ
451 treatment even in immunocompromised mice were striking. Treatment resulted in control
452 in mice that are extremely susceptible to cryptosporidiosis [7, 9] and lack central elements
453 of innate and adaptive immunity. Treatment of immunocompromised individuals suffering
454 from cryptosporidiosis remains very challenging [86, 87]. Clinical trials for use of
455 pegylated IFNλ have shown promise for the treatment of viral infections [88, 89] and its
456 efficacy against *Cryptosporidium* warrants further study.
457

Materials and Methods

Ethics Statement

All *in vivo* experiments were performed in accordance with protocols for animal care approved by the Institutional Animal Care and Use Committee at the University of Pennsylvania (#806292).

Mice

C57/BL6J (stock no: 000664), B6129 (stock no: 101045), Ifng$^{-/-}$ (stock no: 002287), Ifnar$^{-/-}$ (stock no: 028288), Vil1 Cre (stock no: 021504), Mavs$^{-/-}$ (stock no: 008634), Tlr3$^{-/-}$ (stock no: 005217), Tlr7$^{-/-}$ (stock no: 008380) mice were purchased from Jackson Laboratories. C57/BL6 (Model no: B6NTac), Rag2$^{-/-}$ (Model no: RAGN12), Rag2$^{-/-}$ Il2rg$^{-/-}$ (Model no: 4111) mice were purchased from Taconic Biosciences. Vil1-Cre (stock no:021504) were purchased and STAT1flox mice were generated as previously described [90] and maintained in house. Il28ra$^{-/-}$ mice (Bristol Meyers Squibb) were maintained in house. Mice used in this study were males or females between 6-10 weeks of age. All mice were sex and age matched for each experiment. No differences in infection were observed between male and female mice.

Cells, Parasites, and Infections

HCT-8 cells (ATCC) were maintained in RPMI supplemented with 10% FBS at 37°C and 5% CO_2. Wild-type *Cryptosporidium parvum* oocysts used in this study were purchased from Bunchgrass Farms (Dreary, ID). Parasites expressing Tandem mNeon were generated in a previous study [25]. For *in vitro* infections oocysts were incubated in a (1:3)

bleach: water solution for 10 minutes at 4°C, centrifuged then resuspended in a 0.08% solution of sodium deoxytaurocholate and incubated at 16°C for 10 minutes. Oocysts were then washed in PBS and finally resuspended in infection media (complete RPMI with 1% FBS) and added directly to host cells.

C. parvum oocysts used for all *in vivo* experiments are mouse adapted mCherry and Nanoluciferase expressing [14]. Mice were infected with 50,000 *C. parvum* oocysts by oral gavage unless otherwise noted.

Killing Assay

6 well cultures grown to 60% confluency were infected with 5×10^5, 1.25×10^6, 2.5×10^6, 3.75×10^6, or 5×10^6 oocysts per well in biological duplicate. Following a 72-hour infection, cells were trypsinized and incubated in a 1:4 solution of Trypan Blue. Cells were counted and Trypan Blue exclusion used to determine viability.

CRISPR Screen

The Brunello CRISPR sgRNA library [31] was optimized for on-target activity and to minimize off-target effects. Brunello contains four sgRNAs per protein coding gene in the human genome. HCT-8 in media containing 1µg/mL polybrene were spinfected (2 hours, 30°C at 1,000xg) with lentivirus to produce a constitutively expressing Cas9 cell line (lentiCas9-Blast, plasmid#52962, addgene). Following a 7-day selection with blasticidin (1.5µg/mL), cells were diluted to generate clonal Cas9 expressing cell lines. To measure Cas9 activity these cells were subjected to an EGFP reporter assay for Cas9 activity. Cas9 expressing cells were spinfected with lentiXPR_011, encoding an EGFP and a

sgRNA targeting EGFP. 24 hours post spinfection cells were flow sorted to assess green fluorescence. Cells lacking or stably expressing EGFP expressing were used as controls for flow cytometry.

We sought to achieve 1000-fold coverage across multiple biological replicates of the screen. Each replicate achieved 500-fold coverage. Per mL of the Brunello library there were 4.2×10^7 lentiviruses/guides. We infected at an MOI of 0.4 therefore 1.02×10^8 cells were transduced with the library. These cells were trypsinized and spinfected as before into a total of six 6-well plates. Plates were incubated at 37°C, 5% CO2 for 24 hours then media was changed to include 1ug/mL puromycin for selection of transduced cells. Seven days later, cells were trypsinized and expanded into 12 T-175 flasks. After expansion, genomic DNA was isolated from four flasks as the input population and at least 4×10^7 cells (500-fold coverage) were passaged into 4 T-175. These 4 T-175 were then infected with a 90% kill dose of *C. parvum* oocysts. After 72 hours media was replaced with fresh media and cells were allowed to recover. Once confluent, cells were trypsinized and seeded into new flasks to be re-infected while at least 4×10^7 cells were taken for genomic DNA extraction. In total, the population was subjected to three rounds of successive *C. parvum* infection.

Genomic DNA was extracted using the QIAamp DNA Blood Maxi kit (Qiagen). sgRNAs were amplified by PCR as described [31]. Read counts were normalized to reads per million in each condition.

527 **MAGeCK Analysis of CRISPR Screen**

528 Data from our CRISPR screen was analyzed using MAGeCKFlute in R [91]. MAGeCK
529 uses a negative binomial to test for differences in sgRNA abundance between conditions
530 [32]. The input population for Clone K was compared to the output of each round of
531 infection. For Clones C and I input was compared only to the final population. Results
532 shown are for the combined data of screens with Clone I and K. Clone C was excluded
533 due to poor sequencing depth. Genes with three or four sgRNAs positively ranked by the
534 robust ranking aggregation (RRA) algorithm and an FDR of less than 0.05 were
535 considered significantly enriched. Pathways identified by GSEA that included multiple
536 genes of the top candidates were displayed in Fig 1.

537

538 **RNAi Screen**

539 siRNAs targeting top screening candidates were purchased from Ambion (ThermoFisher
540 Scientific, Waltham, MA). Both scrambled non-targeting siRNAs and a positive
541 transfection control RNA targeting GAPDH were included. siRNAs were delivered to 96
542 wells at 50% confluency using Lipofectamine RNAiMax (ThermoFisher Scientific,
543 Waltham, MA) to a final concentration of 100nM per well. 24 hours later, wells were
544 infected with 25,000 *C. parvum* oocysts. At 48 hours post infection, cells were lysed and
545 RNA extracted using the Rneasy Mini Kit (Qiagen). Knockdown of target genes was
546 assessed by qPCR. Host cell viability was measured by MTT (3-(4,5-dimethylthiazol-2-
547 yl)-2,5-diphenyltetrazolium bromide) assay. Briefly, media was removed from all wells
548 and replaced with 100µL of fresh RPMI. 10µL of 12mM MTT solution was added to each
549 well. Plates were incubated at 37°C for 4 hours. Then all media was removed and

replaced with 50µL of DMSO (Sigma, St. Louis, MO) and mixed thoroughly by pipetting up and down. Following a 10 minute incubation at 37°C, plates were read for absorbance at 540nm.

Immunofluorescence assay

Infected HCT-8 coverslip cultures were fixed in 4% paraformaldehyde and permeabilized with 0.1% Triton X-100 for 10 minutes each at room temperature. Samples were blocked in 3% Bovine Serum Albumin (BSA) for 1 hour and primary antibodies were diluted in 3% BSA. Anti-CD151 (ab33315, Abcam) was diluted 1:100 and anti-Tryptophan synthase beta [40] was diluted 1:1000. Secondary antibodies (ThermoFisher) were diluted 1:1000 in 3% BSA. FITC conjugated phalloidin (F432, ThermoFisher) was included in the secondary antibody incubation. Cell nuclei were labeled with Hoechst 1:10,000 for 5 minutes and coverslips were mounted using Vectashield (Vector Laboratories). Slides were imaged using a Leica DM6000 Widefield microscope.

RNA sequencing

Total RNA was extracted using the RNeasy Mini (48-hour) RNeasy Micro (10-hour) kit (Qiagen). cDNA was synthesized using the SMART-Seq v4 Ultra Low Input RNA Kit (Takara Bio USA), and barcoded libraries were prepared using the Nextera XT DNA Library Preparation Kit (Illumina). Total RNA and libraries were quality checked and quantified on an Agilent Tapestation 4200 (Agilent Technologies). Samples were pooled, and single-end reads were run on a NextSeq 500 (Illumina).

572 Reads were pseudo-aligned to the Ensembl *Homo sapiens* reference transcriptome v86
573 using kallisto v0.44.0 [92]. In R, transcripts were collapsed to genes using Bioconductor
574 tximport [93] and differentially expressed genes were identified using Limma-Voom [94,
575 95]. Gene set enrichment analysis (GSEA) was performed using the GSEA software and
576 the annotated gene sets of the Molecular Signatures Database (MSigDB) [96].
577
578 **qPCR**
579 RNA concentrations were measured by NanoDrop (ND-1000; Thermo Fisher Scientific,
580 Waltham, MA) for each sample and an equal amount of cDNA was prepared using
581 SuperScript IV Reverse Transcriptase (Thermo Fisher Scientific, Waltham, MA).
582 Following reverse transcription, a 20µL reaction was loaded into a ViiA 7 Real Time PCR
583 system (Thermo Fisher Scientific, Waltham, MA). The following conditions were used:
584 Initial incubation 3 min at 95°C, 40 cycles of 95°C for 15 sec and 60°C for 30 sec. A single
585 melt curve and ΔΔCt method was used to determine relative expression with GAPDH
586 used as the housekeeping gene. See Table 1 for list of primers.
587
588 **Western Blot**
589 24 well HCT-8 cultures grown to 60% confluency were infected with $2x10^5$ C. parvum
590 oocysts in RPMI containing 1% serum for the indicated time. Media was removed and
591 cells were lysed in Pierce™ IP Lysis Buffer (ThermoFisher Scientific, Waltham, MA),
592 supplemented 1:100 with protease inhibitor cocktail (Sigma St. Louis, MO). Lysates were
593 incubated on ice 10 minutes, then spun at 20,000 g for 10 min at 4°C. The cleared lysate
594 was removed and flash frozen. Cleared lysates were thawed on ice and protein

concentration was assessed by BCA (23225, ThermoFisher Scientific, Waltham, MA). 18µg of sample was loaded per well diluted 1:1 with freshly prepared 2X Laemmli Sample buffer (BioRad Hercules, CA) + β-Mercaptoethanol (1:20) (Sigma St. Louis, MO) and boiled for 10 minutes at 95°C. 20 µL sample was loaded per each lane of an any KD Mini-PROTEAN® TGX™ Precast Protein Gel (BioRad Hercules, CA) and run at 150 V for 1 hour. Wet transfer to a 0.45 µm pore size pre-cut Nitrocellulose membrane (ThermoFisher Scientific Waltham, MA) was conducted at 20V for 2.5 hours at room temperature. The Nitrocellulose membrane was blocked for 1 hour at room temperature using Intercept®(TBS) Protein-Free Blocking Buffer (LI-COR Lincoln, NE). Primary antibody was incubated at room temperature for 2 hours in Intercept®(TBS) Protein-Free Blocking Buffer with 0.01% Tween®20 (Sigma, St. Louis, MO) using STAT1 1:1000 (#14994, Cell Signaling Technology), phosphor STAT1 Y701 1:1000 (ab29045, Abcam) and alpha-tubulin 1:5000 (ab7291, Abcam). The membrane was washed 3 times with PBS with 0.01% Tween®20 (Sigma, St. Louis, MO). Secondary antibody was incubated at room temperature protected from light for 1 hour in Intercept®(TBS) Protein-Free Blocking Buffer with 0.01% Tween®20 (Sigma, St. Louis, MO) using IRDye® 800CW Goat anti-Mouse IgG secondary antibody at 1:10,000 (LI-COR Lincoln, NE) and IRDye® 680RD Goat anti-Rabbit IgG secondary antibody at 1:10,000 (LI-COR, Lincoln, NE). After 3 PBS + 0.01% Tween®20 (Sigma, St. Louis, MO) washes, the membrane was imaged on the Odyssey Infrared Imaging System v3.0 (LICOR, Lincoln, NE).

ELISA

96 well HCT-8 cultures grown to 60% confluency were infected with 25,000 *C. parvum* oocysts. At the indicated timepoint post infection, supernatants were removed and spun at 1,000xg for 10 minutes to pellet debris. Supernatants were frozen at -80°C. IFNβ and IFNλ protein levels from HCT-8 cultures were measured by Human IFN-beta DuoSet ELISA (DY814, R&D Systems) and Human IL29/IL28B (IFN-lambda 1/3) DuoSet ELISA (DY1598B, R&D Systems). Protein levels of IFNλ from intestinal biopsies were measured by Mouse IL28B/ IFN-lambda 3 DuoSet ELISA (DY1789B, R&D Systems). Protein levels of IL-18 from intestinal biopsies were measured by ELISA (BMS618-3, ThermoFisher, Waltham, MA). Assays were performed according to the manufacturer's instructions.

Flow sorting of infected cells

HCT-8 6 well cultures were infected with $1x10^6$ *C. parvum* Neon oocysts. 10 hours later, cells were trypsinized in TrypLE (ThermoFisher), washed with PBS, and passed through a 40 µm filter. Cells were sorted using a BD FACSJazz Sorter (BD Biosciences). Uninfected HCT-8 were used to gate on singlets. 10,000 positive cells and 10,000 negative cells were sorted from three independent biological replicates directly into RLT Lysis buffer (Qiagen).

Ileal biopsies

Three 5mm punch biopsies were taken from the distal small intestine of each mouse. Punches were incubated in complete RPMI for 18 hours. Supernatants were then used for ELISA.

For qPCR, punches were placed in RNAlater (Sigma) at 4°C until RNA was extracted using the RNeasy Mini Kit (Qiagen)

Nanoluciferase Assay

To monitor infection *in vivo*, 20mg of fecal material was resuspended in 1mL of lysis buffer. Samples were shaken with glass beads for 5min at 2,000 rpm. Samples were briefly centrifuged to pellet any floating material and the cleared lysate was mixed 1:1 with prepared Nanoluciferase solution (substrate: lysis buffer 1:50). Luminescence was measured using a Promega GloMax plate reader.

Cytokine neutralization and administration

To neutralize IFNλ, 20µg of Anti IL28A/B (Clone 244716, MAB17892, R&D Systems, Minneapolis, MN) was infected intraperitoneally one day prior and each day following infection for the duration.

For administration of Ifnλ2 (250-33, Peprotech, Cranbury, NJ), 1µg, unless otherwise noted, was injected intraperitoneally daily beginning at 6-8 hours prior to infection and then each day of the infection.

Histology

Tissue from the lower third of the small intestine was flushed with 10% neutral buffered formalin (Sigma, St Louis, MO, USA), then ‘swiss-rolled’ and fixed overnight. Fixed samples were paraffin-embedded, sectioned, and stained with hematoxylin and eosin for detailed histologic evaluation. Slides were evaluated by a board-certified veterinary

664 pathologist in a blinded fashion for quantitative measurements of number of parasites,
665 villus/crypt architectural features, and semi-quantitative scores for villus epithelium
666 lesions as previously described [97].
667
668 **PRR agonist screen**
669 Agonists of pattern recognition receptors were purchased from Invivogen. Cells were
670 seeded into 96 well plates and at 60% confluency, cells were either infected with C.
671 parvum (25,000 oocysts per well) or treated with an agonist. 10µg/mL LMW Poly (I:C)
672 was either lipofected or added to the medium. The following agonists were delivered with
673 Lipofectamine: 5'ppp RNA (10µg/mL), mTriDAP (10µg/mL), HSV60 (5µg/mL), ssPolyU
674 RNA (10µg/mL), and CpG ODN (5µM). After 24 hours the media was removed for ELISA
675 and the cells were lysed and RNA extracted (RNeasy Mini Kit, Qiagen).
676
677 **Statistical Methods**
678 Mean +/- SD are reported. When measuring the difference between two populations, a
679 standard *t*-test was used. For datasets with 3 or more experimental groups, a one-way
680 ANOVA with multiple comparison's test was used. For datasets with 2 or more
681 experimental groups and an additional factor of time, a two-way ANOVA with multiple
682 comparison's test was used and simple linear regression was used to determine the
683 goodness of fit curve for host cell killing by *C. parvum*. *P* values of less than 0.05 were
684 considered significant. These tests were performed in GraphPad Prism or in R.
685
686

Data Availability

Data are within the manuscript and supporting information files and are accessible through GEO accession number: GSE185247. All code used to process and analyze the data is available through Code Ocean: https://doi.org/10.24433/CO.1074647.v1

References

1. Hlavsa MC, Cikesh BL, Roberts VA, Kahler AM, Vigar M, Hilborn ED, et al. Outbreaks Associated with Treated Recreational Water - United States, 2000-2014. MMWR Morb Mortal Wkly Rep. 2018;67(19):547-51.
2. Colford JM, Jr., Tager IB, Hirozawa AM, Lemp GF, Aragon T, Petersen C. Cryptosporidiosis among Patients Infected with Human Immunodeficiency Virus: Factors Related to Symptomatic Infection and Survival. American Journal of Epidemiology. 1996;144(9):807-16.
3. Kotloff KL, Nataro JP, Blackwelder WC, Nasrin D, Farag TH, Panchalingam S, et al. Burden and aetiology of diarrhoeal disease in infants and young children in developing countries (the Global Enteric Multicenter Study, GEMS): a prospective, case-control study. The Lancet. 2013;382(9888):209-22.
4. Kabir M, Alam M, Nayak U, Arju T, Hossain B, Tarannum R, et al. Nonsterile immunity to cryptosporidiosis in infants is associated with mucosal IgA against the sporozoite and protection from malnutrition. PLOS Pathogens. 2021;17(6):e1009445.
5. Ungar BL, Kao TC, Burris JA, Finkelman FD. Cryptosporidium infection in an adult mouse model. Independent roles for IFN-gamma and CD4+ T lymphocytes in protective immunity. The Journal of Immunology. 1991;147(3):1014.
6. Chen W, Harp JA, Harmsen AG, Havell EA. Gamma interferon functions in resistance to Cryptosporidium parvum infection in severe combined immunodeficient mice. Infection and Immunity. 1993;61(8):3548-51.
7. Barakat FM, McDonald V, Di Santo JP, Korbel DS. Roles for NK Cells and an NK Cell-Independent Source of Intestinal Gamma Interferon for Innate Immunity to Cryptosporidium parvum Infection. Infection and Immunity. 2009;77(11):5044-9.
8. Pollok RCG, Farthing MJG, Bajaj-Elliott M, Sanderson IR, McDonald V. Interferon gamma induces enterocyte resistance against infection by the intracellular pathogen Cryptosporidium parvum. Gastroenterology. 2001;120(1):99-107.
9. Gullicksrud J, Sateriale A, Engiles J, Gibson AR, Shaw S, Hutchins Z, et al. Enterocyte–ILC1 crosstalk drives innate IFNg mediated control of Cryptosporidium. Mucosal Immunology. 2021:Forthcoming.
10. Laurent F, Eckmann L, Savidge TC, Morgan G, Theodos C, Naciri M, et al. Cryptosporidium parvum infection of human intestinal epithelial cells induces the polarized secretion of C-X-C chemokines. Infection and Immunity. 1997;65(12):5067-73.
11. Maillot C, Gargala G, Delaunay A, Ducrotte P, Brasseur P, Ballet JJ, et al. Cryptosporidium parvum infection stimulates the secretion of TGF-β, IL-8 and RANTES by Caco-2 cell line. Parasitology Research. 2000;86(12):947-9.
12. Ferguson SH, Foster DM, Sherry B, Magness ST, Nielsen DM, Gookin JL. Interferon-Lambda Promotes Epithelial Defense and Barrier Function Against Cryptosporidium parvum Infection. Cellular and Molecular Gastroenterology and Hepatology. 2019;8(1):1-20.
13. Barakat FM, McDonald V, Foster GR, Tovey MG, Korbel DS. Cryptosporidium parvum Infection Rapidly Induces a Protective Innate Immune Response Involving Type I Interferon. The Journal of Infectious Diseases. 2009;200(10):1548-55.
14. Sateriale A, Gullicksrud JA, Engiles JB, McLeod BI, Kugler EM, Henao-Mejia J, et al. The intestinal parasite Cryptosporidium is controlled by an enterocyte intrinsic

inflammasome that depends on NLRP6. Proceedings of the National Academy of Sciences. 2021;118(2):e2007807118.
15. Heo I, Dutta D, Schaefer DA, Iakobachvili N, Artegiani B, Sachs N, et al. Modelling Cryptosporidium infection in human small intestinal and lung organoids. Nature Microbiology. 2018;3(7):814-23.
16. Nikolaev M, Mitrofanova O, Broguiere N, Geraldo S, Dutta D, Tabata Y, et al. Homeostatic mini-intestines through scaffold-guided organoid morphogenesis. Nature. 2020;585(7826):574-8.
17. Pott J, Stockinger S. Type I and III Interferon in the Gut: Tight Balance between Host Protection and Immunopathology. Frontiers in Immunology. 2017;8(258).
18. Sponseller JK, Griffiths JK, Tzipori S. The Evolution of Respiratory Cryptosporidiosis: Evidence for Transmission by Inhalation. Clinical Microbiology Reviews. 2014;27(3):575-86.
19. Vakil NB, Schwartz SM, Buggy BP, Brummitt CF, Kherellah M, Letzer DM, et al. Biliary Cryptosporidiosis in HIV-Infected People after the Waterborne Outbreak of Cryptosporidiosis in Milwaukee. New England Journal of Medicine. 1996;334(1):19-23.
20. Elliott David A, Clark Douglas P. Cryptosporidium parvum Induces Host Cell Actin Accumulation at the Host-Parasite Interface. Infection and Immunity. 2000;68(4):2315-22.
21. Current WL, Reese NC. A Comparison of Endogenous Development of Three Isolates of Cryptosporidium in Suckling Mice. The Journal of Protozoology. 1986;33(1):98-108.
22. Kumar A, Chatterjee I, Anbazhagan AN, Jayawardena D, Priyamvada S, Alrefai WA, et al. Cryptosporidium parvum disrupts intestinal epithelial barrier function via altering expression of key tight junction and adherens junction proteins. Cellular Microbiology. 2018;20(6):e12830.
23. Chen X-M, Huang BQ, Splinter PL, Cao H, Zhu G, McNiven MA, et al. Cryptosporidium parvum invasion of biliary epithelia requires host cell tyrosine phosphorylation of cortactin via c-Src. Gastroenterology. 2003;125(1):216-28.
24. Guérin A, Roy NH, Kugler EM, Berry L, Burkhardt JK, Shin J-B, et al. Cryptosporidium rhoptry effector protein ROP1 injected during invasion targets the host cytoskeletal modulator LMO7. Cell Host & Microbe. 2021.
25. Dumaine JE, Sateriale A, Gibson AR, Reddy A, Gullicksrud J, Hunter E, et al. The diarrheal pathogen Cryptosporidium parvum exports proteins into the cytoplasm of the infected host cell. eLife. 2021:Forthcoming.
26. Guérin A, Striepen B. The Biology of the Intestinal Intracellular Parasite Cryptosporidium. Cell Host & Microbe. 2020;28(4):509-15.
27. Chen X-M, O'Hara SP, Huang BQ, Nelson JB, Lin JJ-C, Zhu G, et al. Apical Organelle Discharge by Cryptosporidium parvum Is Temperature, Cytoskeleton, and Intracellular Calcium Dependent and Required for Host Cell Invasion. Infection and Immunity. 2004;72(12):6806-16.
28. Upton SJ, Tilley M, Brillhart DB. Comparative development of Cryptosporidium parvum (Apicomplexa) in 11 continuous host cell lines. FEMS Microbiology Letters. 1994;118(3):233-6.
29. Sanjana NE, Shalem O, Zhang F. Improved vectors and genome-wide libraries for CRISPR screening. Nat Meth. 2014;11(8):783-4.

30. Doench JG, Hartenian E, Graham DB, Tothova Z, Hegde M, Smith I, et al. Rational design of highly active sgRNAs for CRISPR-Cas9–mediated gene inactivation. Nature Biotechnology. 2014;32(12):1262-7.
31. Doench JG, Fusi N, Sullender M, Hegde M, Vaimberg EW, Donovan KF, et al. Optimized sgRNA design to maximize activity and minimize off-target effects of CRISPR-Cas9. Nature Biotechnology. 2016;34(2):184-91.
32. Li W, Xu H, Xiao T, Cong L, Love MI, Zhang F, et al. MAGeCK enables robust identification of essential genes from genome-scale CRISPR/Cas9 knockout screens. Genome Biology. 2014;15(12):554.
33. Gomez Morales MA, Ausiello CM, Guarino A, Urbani F, Spagnuolo MI, Pignata C, et al. Severe, Protracted Intestinal Cryptosporidiosis Associated with Interferon γ Deficiency: Pediatric Case Report. Clinical Infectious Diseases. 1996;22(5):848-50.
34. Bierne H, Travier L, Mahlakõiv T, Tailleux L, Subtil A, Lebreton A, et al. Activation of Type III Interferon Genes by Pathogenic Bacteria in Infected Epithelial Cells and Mouse Placenta. PLOS ONE. 2012;7(6):e39080.
35. Crotta S, Davidson S, Mahlakoiv T, Desmet CJ, Buckwalter MR, Albert ML, et al. Type I and Type III Interferons Drive Redundant Amplification Loops to Induce a Transcriptional Signature in Influenza-Infected Airway Epithelia. PLOS Pathogens. 2013;9(11):e1003773.
36. Tandel J, English ED, Sateriale A, Gullicksrud JA, Beiting DP, Sullivan MC, et al. Life cycle progression and sexual development of the apicomplexan parasite Cryptosporidium parvum. Nature Microbiology. 2019;4(12):2226-36.
37. Odendall C, Voak AA, Kagan JC. Type III IFNs Are Commonly Induced by Bacteria-Sensing TLRs and Reinforce Epithelial Barriers during Infection. The Journal of Immunology. 2017;199(9):3270.
38. Yoshimura A, Lien E, Ingalls RR, Tuomanen E, Dziarski R, Golenbock D. Cutting Edge: Recognition of Gram-Positive Bacterial Cell Wall Components by the Innate Immune System Occurs Via Toll-Like Receptor 2. The Journal of Immunology. 1999;163(1):1.
39. Rusinova I, Forster S, Yu S, Kannan A, Masse M, Cumming H, et al. INTERFEROME v2.0: an updated database of annotated interferon-regulated genes. Nucleic Acids Research. 2012;41(D1):D1040-D6.
40. Vinayak S, Pawlowic MC, Sateriale A, Brooks CF, Studstill CJ, Bar-Peled Y, et al. Genetic modification of the diarrhoeal pathogen Cryptosporidium parvum. Nature. 2015;523(7561):477-80.
41. Gimeno Brias S, Marsden M, Forbester J, Clement M, Brandt C, Harcourt K, et al. Interferon lambda is required for interferon gamma-expressing NK cell responses but does not afford antiviral protection during acute and persistent murine cytomegalovirus infection. PLOS ONE. 2018;13(5):e0197596.
42. Culshaw RJ, Bancroft GJ, McDonald V. Gut intraepithelial lymphocytes induce immunity against Cryptosporidium infection through a mechanism involving gamma interferon production. Infection and Immunity. 1997;65(8):3074-9.
43. Syedbasha M, Egli A. Interferon Lambda: Modulating Immunity in Infectious Diseases. Frontiers in Immunology. 2017;8(119).

826 44. Qiao Y, Zhu S, Deng S, Zou S-S, Gao B, Zang G, et al. Human Cancer Cells
827 Sense Cytosolic Nucleic Acids Through the RIG-I–MAVS Pathway and cGAS–STING
828 Pathway. Frontiers in Cell and Developmental Biology. 2021;8(1668).
829 45. Broz P, Monack DM. Newly described pattern recognition receptors team up
830 against intracellular pathogens. Nature Reviews Immunology. 2013;13(8):551-65.
831 46. Bedi B, McNair NN, Forster I, Mead JR. IL-18 cytokine levels modulate innate
832 immune responses and cryptosporidiosis in mice. J Eukaryot Microbiol. 2015;62(1):44-
833 50.
834 47. Sateriale A, Gullicksrud JA, Engiles JB, McLeod BI, Kugler EM, Henao-Mejia J,
835 et al. The intestinal parasite Cryptosporidium is controlled by an enterocyte intrinsic
836 inflammasome that depends on NLRP6. Proc Natl Acad Sci U S A. 2021;118(2).
837 48. Ludington JG, Ward HD, Adams JH. The Cryptosporidium parvum C-Type Lectin
838 CpClec Mediates Infection of Intestinal Epithelial Cells via Interactions with Sulfated
839 Proteoglycans. Infection and Immunity. 2016;84(5):1593-602.
840 49. Lisanti M, Le Bivic A, Saltiel A, Rodriguez-Boulan E. Preferred apical distribution
841 of glycosyl-phosphatidylinositol (GPI) anchored proteins: A highly conserved feature of
842 the polarized epithelial cell phenotype. The Journal of membrane biology.
843 1990;113:155-67.
844 50. Filmus J, Capurro M, Rast J. Glypicans. Genome Biol. 2008;9(5):224.
845 51. Fast LA, Lieber D, Lang T, Florin L. Tetraspanins in infections by human
846 cytomegalo- and papillomaviruses. Biochem Soc T. 2017;45:489-97.
847 52. Silvie O, Rubinstein E, Franetich JF, Prenant M, Belnoue E, Renia L, et al.
848 Hepatocyte CD81 is required for Plasmodium falciparum and Plasmodium yoelii
849 sporozoite infectivity. Nature Medicine. 2003;9(1):93-6.
850 53. Termini CM, Gillette JM. Tetraspanins Function as Regulators of Cellular
851 Signaling. Frontiers in Cell and Developmental Biology. 2017;5(34).
852 54. Li Y, Yang J, Wang H, Qiao W, Guo Y, Zhang S, et al. FNDC3B, Targeted by
853 miR-125a-5p and miR-217, Promotes the Proliferation and Invasion of Colorectal
854 Cancer Cells via PI3K/mTOR Signaling. Onco Targets Ther. 2020;13:3501-10.
855 55. Zhang H, Guo F, Zhu G, Urban JF. Involvement of Host Cell Integrin α2 in
856 Cryptosporidium parvum Infection. Infection and Immunity. 2012;80(5):1753-8.
857 56. Chen X-M, Splinter PL, Tietz PS, Huang BQ, Billadeau DD, LaRusso NF.
858 Phosphatidylinositol 3-Kinase and Frabin Mediate Cryptosporidium parvum
859 Cellular Invasion via Activation of Cdc42 *. Journal of Biological Chemistry.
860 2004;279(30):31671-8.
861 57. Rauch I, Deets KA, Ji DX, von Moltke J, Tenthorey JL, Lee AY, et al. NAIP-
862 NLRC4 Inflammasomes Coordinate Intestinal Epithelial Cell Expulsion with Eicosanoid
863 and IL-18 Release via Activation of Caspase-1 and -8. Immunity. 2017;46(4):649-59.
864 58. Nousiainen L, Sillanpää M, Jiang M, Thompson J, Taipale J, Julkunen I. Human
865 kinome analysis reveals novel kinases contributing to virus infection and retinoic-acid
866 inducible gene I-induced type I and type III IFN gene expression. Innate Immunity.
867 2013;19(5):516-30.
868 59. Johnsen IB, Nguyen TT, Bergstroem B, Fitzgerald KA, Anthonsen MW. The
869 Tyrosine Kinase c-Src Enhances RIG-I (Retinoic Acid-inducible Gene I)-elicited Antiviral
870 Signaling *. Journal of Biological Chemistry. 2009;284(28):19122-31.

60. Shirakawa R, Horiuchi H. Ral GTPases: crucial mediators of exocytosis and tumourigenesis. The Journal of Biochemistry. 2015;157(5):285-99.
61. Nichols CD, Casanova JE. Salmonella-Directed Recruitment of New Membrane to Invasion Foci via the Host Exocyst Complex. Current Biology. 2010;20(14):1316-20.
62. Bryde S, Hennrich H, Verhulst PM, Devaux PF, Lenoir G, Holthuis JCM. CDC50 Proteins Are Critical Components of the Human Class-1 P₄-ATPase Transport Machinery *. Journal of Biological Chemistry. 2010;285(52):40562-72.
63. Yang Y, Sun K, Liu W, Li X, Tian W, Shuai P, et al. The phosphatidylserine flippase β-subunit Tmem30a is essential for normal insulin maturation and secretion. Molecular Therapy. 2021.
64. Cullinane AR, Schäffer AA, Huizing M. The BEACH Is Hot: A LYST of Emerging Roles for BEACH-Domain Containing Proteins in Human Disease. Traffic. 2013;14(7):749-66.
65. Lukov GL, Hu T, McLaughlin JN, Hamm HE, Willardson BM. Phosducin-like protein acts as a molecular chaperone for G protein βγ dimer assembly. The EMBO Journal. 2005;24(11):1965-75.
66. Harrison T, Samuel BU, Akompong T, Hamm H, Mohandas N, Lomasney JW, et al. Erythrocyte G Protein-Coupled Receptor Signaling in Malarial Infection. Science. 2003;301(5640):1734.
67. Anand-Srivastava MB, Sairam MR, Cantin M. Ring-deleted analogs of atrial natriuretic factor inhibit adenylate cyclase/cAMP system. Possible coupling of clearance atrial natriuretic factor receptors to adenylate cyclase/cAMP signal transduction system. Journal of Biological Chemistry. 1990;265(15):8566-72.
68. Barber GN. The interferons and cell death: guardians of the cell or accomplices of apoptosis? Seminars in Cancer Biology. 2000;10(2):103-11.
69. Schmeisser H, Bekisz J, Zoon KC. New Function of Type I IFN: Induction of Autophagy. Journal of Interferon & Cytokine Research. 2014;34(2):71-8.
70. Brand S, Beigel F, Olszak T, Zitzmann K, Eichhorst ST, Otte J-M, et al. IL-28A and IL-29 mediate antiproliferative and antiviral signals in intestinal epithelial cells and murine CMV infection increases colonic IL-28A expression. American Journal of Physiology-Gastrointestinal and Liver Physiology. 2005;289(5):G960-G8.
71. Gao Z, Zhu M, Wu Y, Gao P, Qin Z, Wang H. Interferon-λ1 induces G1 phase cell cycle arrest and apoptosis in gastric carcinoma cells in vitro. Oncol Rep. 2014;32(1):199-204.
72. Maher SG, Sheikh F, Scarzello AJ, Romero-Weaver AL, Baker DP, Donnelly RP, et al. IFN-α and IFN-λ differ in their antiproliferative effects and duration of JAK/STAT signaling activity. Cancer Biology & Therapy. 2008;7(7):1109-15.
73. Jarry A, Malard F, Bou-Hanna C, Meurette G, Mohty M, Mosnier J-F, et al. Interferon-Alpha Promotes Th1 Response and Epithelial Apoptosis via Inflammasome Activation in Human Intestinal Mucosa. Cellular and Molecular Gastroenterology and Hepatology. 2017;3(1):72-81.
74. Lantier L, Drouet F, Guesdon W, Mancassola R, Metton C, Lo-Man R, et al. Poly(I:C)-Induced Protection of Neonatal Mice Against Intestinal Cryptosporidium parvum Infection Requires an Additional TLR5 Signal Provided by the Gut Flora. The Journal of Infectious Diseases. 2013;209(3):457-67.

75. Beiting DP, Peixoto L, Akopyants NS, Beverley SM, Wherry EJ, Christian DA, et al. Differential Induction of TLR3-Dependent Innate Immune Signaling by Closely Related Parasite Species. PLOS ONE. 2014;9(2):e88398.
76. Ives A, Ronet C, Prevel F, Ruzzante G, Fuertes-Marraco S, Schutz F, et al. Leishmania RNA Virus Controls the Severity of Mucocutaneous Leishmaniasis. Science. 2011;331(6018):775-8.
77. Khramtsov NV, Chung PA, Dykstra CC, Griffiths JK, Morgan UM, Arrowood MJ, et al. PRESENCE OF DOUBLE-STRANDED RNAs IN HUMAN AND CALF ISOLATES OF CRYPTOSPORIDIUM PARVUM. Journal of Parasitology. 2000;86(2):275-82.
78. Khramtsov NV, Woods KM, Nesterenko MV, Dykstra CC, Upton SJ. Virus-like, double-stranded RNAs in the parasitic protozoan Cryptosporidium parvum. Molecular Microbiology. 1997;26(2):289-300.
79. de Carvalho RVH, Lima-Junior DS, da Silva MVG, Dilucca M, Rodrigues TS, Horta CV, et al. Leishmania RNA virus exacerbates Leishmaniasis by subverting innate immunity via TLR3-mediated NLRP3 inflammasome inhibition. Nature Communications. 2019;10(1):5273.
80. Wang Y, Gong A-Y, Ma S, Chen X, Li Y, Su C-J, et al. Delivery of Parasite RNA Transcripts Into Infected Epithelial Cells During Cryptosporidium Infection and Its Potential Impact on Host Gene Transcription. The Journal of Infectious Diseases. 2016;215(4):636-43.
81. Lee BL, Moon JE, Shu JH, Yuan L, Newman ZR, Schekman R, et al. UNC93B1 mediates differential trafficking of endosomal TLRs. eLife. 2013;2:e00291.
82. Pott J, Stockinger S, Torow N, Smoczek A, Lindner C, McInerney G, et al. Age-Dependent TLR3 Expression of the Intestinal Epithelium Contributes to Rotavirus Susceptibility. PLOS Pathogens. 2012;8(5):e1002670.
83. Schulz O, Diebold SS, Chen M, Näslund TI, Nolte MA, Alexopoulou L, et al. Toll-like receptor 3 promotes cross-priming to virus-infected cells. Nature. 2005;433(7028):887-92.
84. Kato H, Takeuchi O, Sato S, Yoneyama M, Yamamoto M, Matsui K, et al. Differential roles of MDA5 and RIG-I helicases in the recognition of RNA viruses. Nature. 2006;441(7089):101-5.
85. Lantier L, Lacroix-Lamandé S, Potiron L, Metton C, Drouet F, Guesdon W, et al. Intestinal CD103+ Dendritic Cells Are Key Players in the Innate Immune Control of Cryptosporidium parvum Infection in Neonatal Mice. PLOS Pathogens. 2013;9(12):e1003801.
86. Huston CD. The Clofazimine for Treatment of Cryptosporidiosis in HIV-Infected Adults (CRYPTOFAZ) and Lessons Learned for Anticryptosporidial Drug Development. Clinical Infectious Diseases. 2020;73(2):192-4.
87. Hadžić N, Nademi Z, Deheragoda M, Zen Y, Elfeky R, Worth A, et al. Chronic Cholangiopathy Associated with Primary Immune Deficiencies Can Be Resolved by Effective Hematopoietic Stem Cell Transplantation. The Journal of Pediatrics. 2019;209:97-106.e2.
88. Feld JJ, Kandel C, Biondi MJ, Kozak RA, Zahoor MA, Lemieux C, et al. Peginterferon lambda for the treatment of outpatients with COVID-19: a phase 2, placebo-controlled randomised trial. The Lancet Respiratory Medicine. 2021;9(5):498-510.

962 89. Phillips S, Mistry S, Riva A, Cooksley H, Hadzhiolova-Lebeau T, Plavova S, et al.
963 Peg-Interferon Lambda Treatment Induces Robust Innate and Adaptive Immunity in
964 Chronic Hepatitis B Patients. Frontiers in Immunology. 2017;8(621).
965 90. Klover PJ, Muller WJ, Robinson GW, Pfeiffer RM, Yamaji D, Hennighausen L.
966 Loss of STAT1 from Mouse Mammary Epithelium Results in an Increased Neu-Induced
967 Tumor Burden. Neoplasia. 2010;12(11):899-905.
968 91. Wang B, Wang M, Zhang W, Xiao T, Chen C-H, Wu A, et al. Integrative analysis
969 of pooled CRISPR genetic screens using MAGeCKFlute. Nature Protocols.
970 2019;14(3):756-80.
971 92. Bray NL, Pimentel H, Melsted P, Pachter L. Near-optimal probabilistic RNA-seq
972 quantification. Nature Biotechnology. 2016;34(5):525-7.
973 93. Robinson MD, McCarthy DJ, Smyth GK. edgeR: a Bioconductor package for
974 differential expression analysis of digital gene expression data. Bioinformatics.
975 2009;26(1):139-40.
976 94. Ritchie ME, Phipson B, Wu D, Hu Y, Law CW, Shi W, et al. limma powers
977 differential expression analyses for RNA-sequencing and microarray studies. Nucleic
978 Acids Res. 2015;43(7):e47.
979 95. Law CW, Chen Y, Shi W, Smyth GK. voom: precision weights unlock linear
980 model analysis tools for RNA-seq read counts. Genome Biology. 2014;15(2):R29.
981 96. Subramanian A, Tamayo P, Mootha VK, Mukherjee S, Ebert BL, Gillette MA, et
982 al. Gene set enrichment analysis: A knowledge-based approach for interpreting
983 genome-wide expression profiles. Proceedings of the National Academy of Sciences.
984 2005;102(43):15545.
985 97. Sateriale A, Šlapeta J, Baptista R, Engiles JB, Gullicksrud JA, Herbert GT, et al.
986 A Genetically Tractable, Natural Mouse Model of Cryptosporidiosis Offers Insights into
987 Host Protective Immunity. Cell Host & Microbe. 2019;26(1):135-46.e5.
988

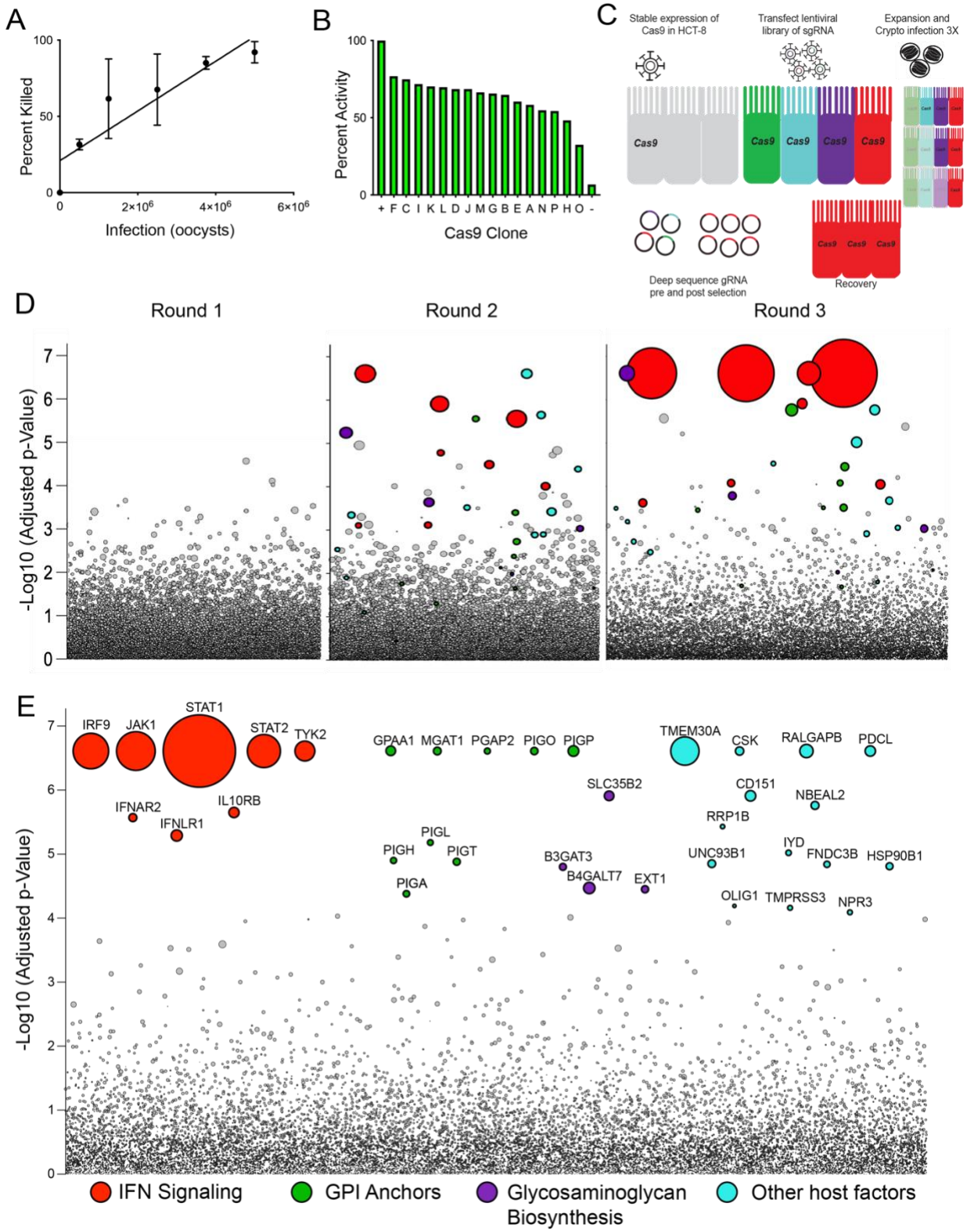

991

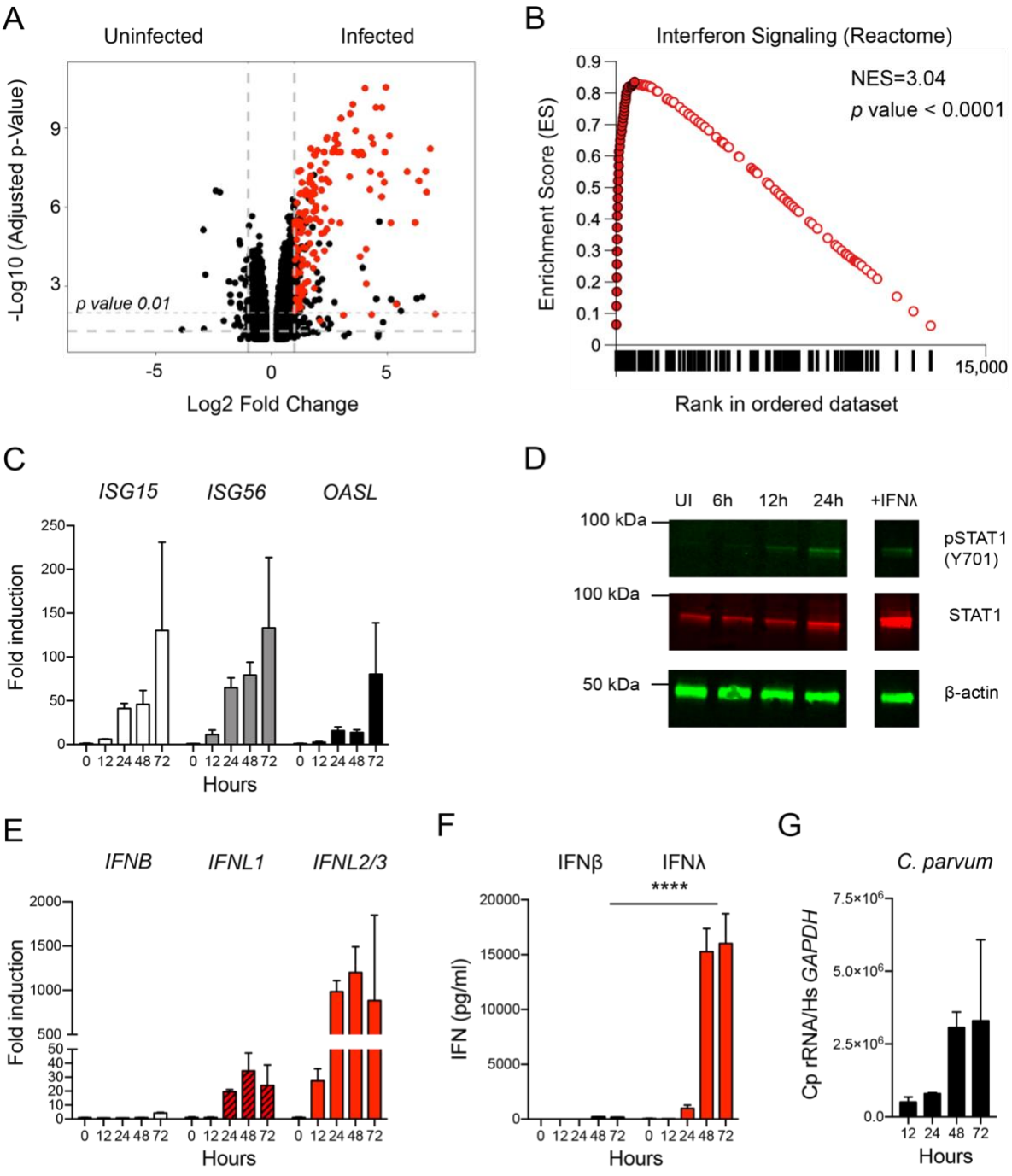

992

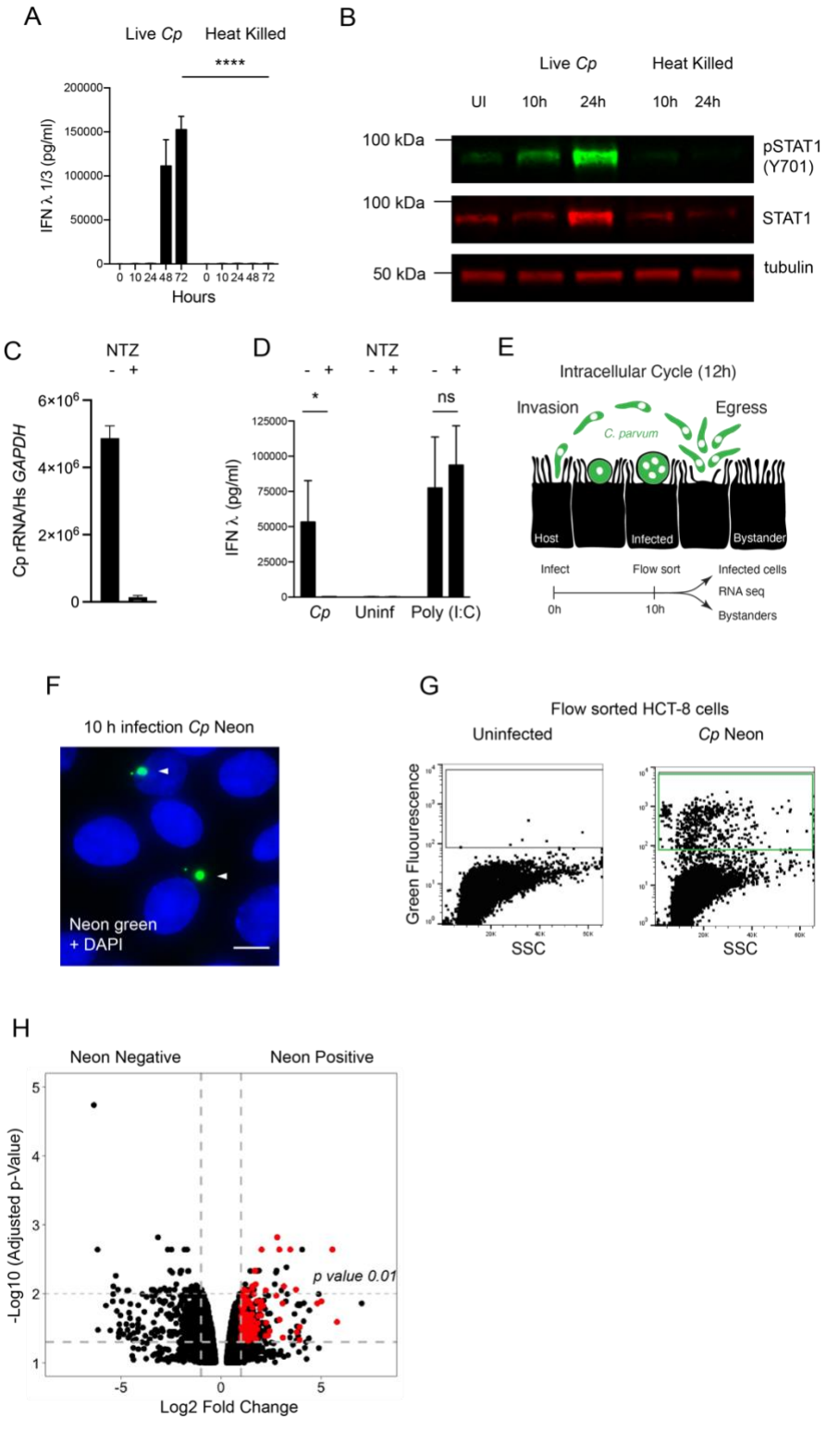

993

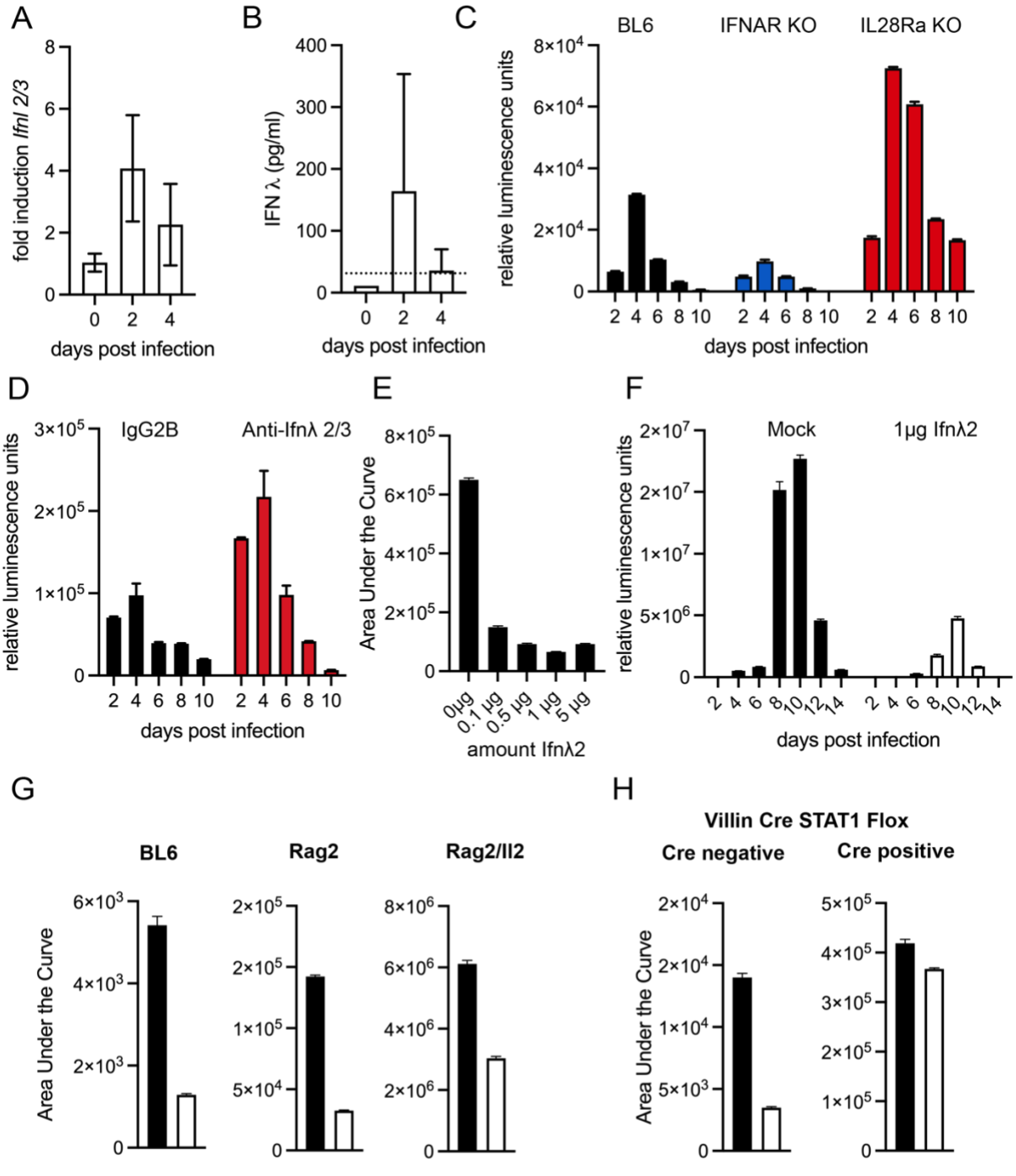

994

995

996

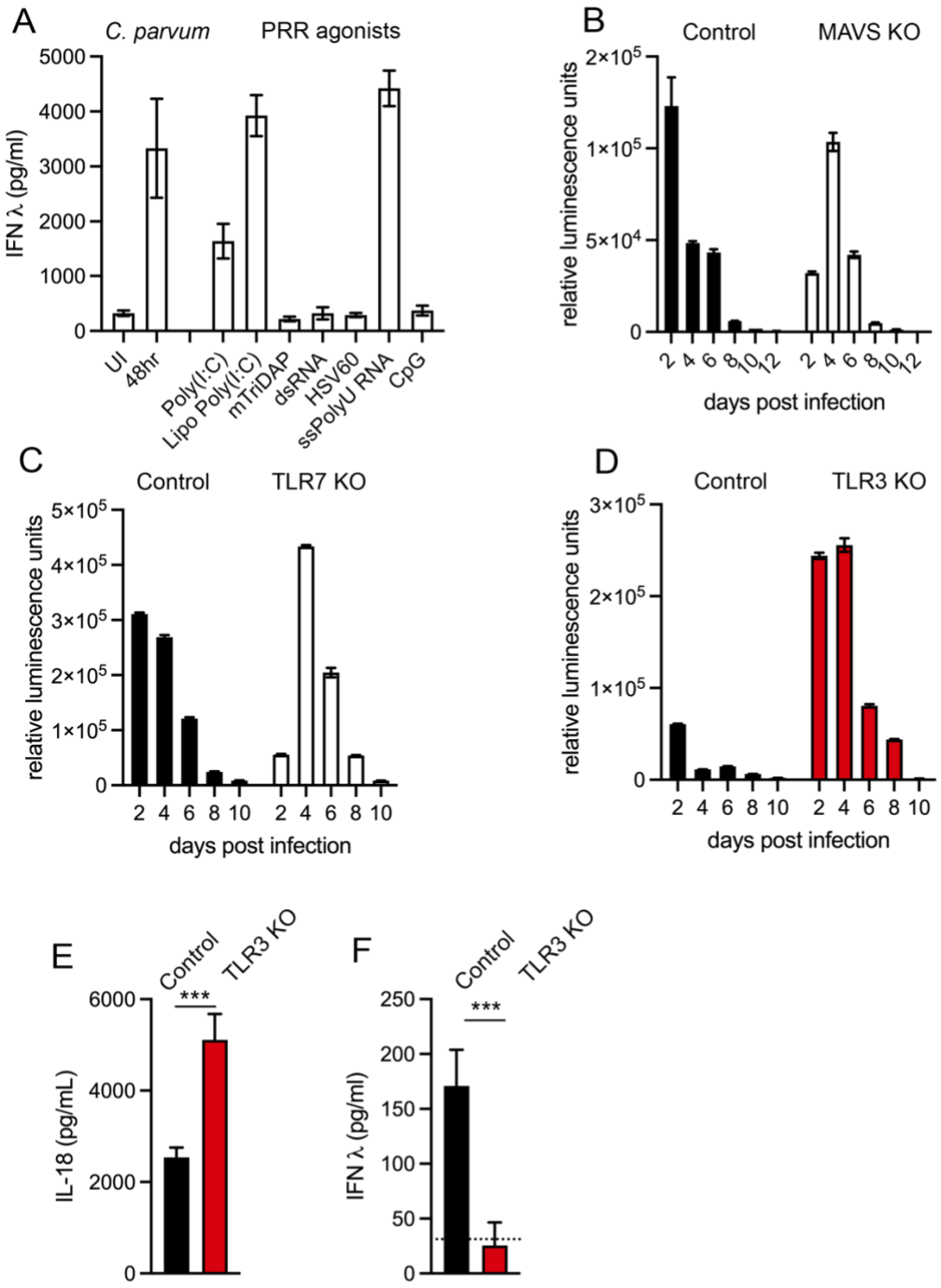

997

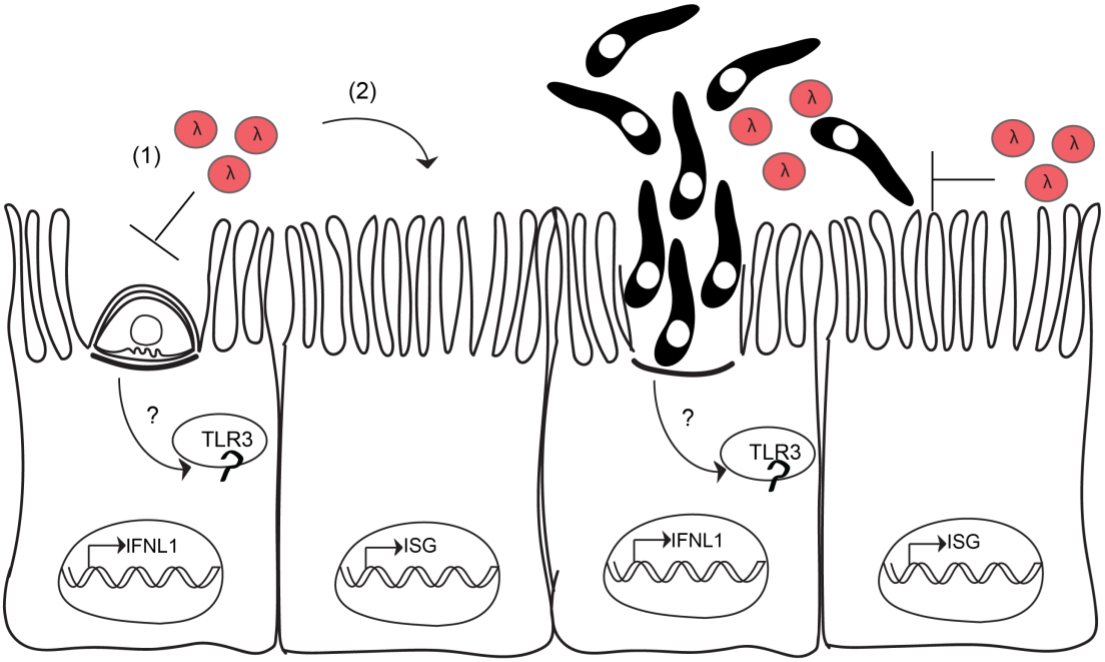

998

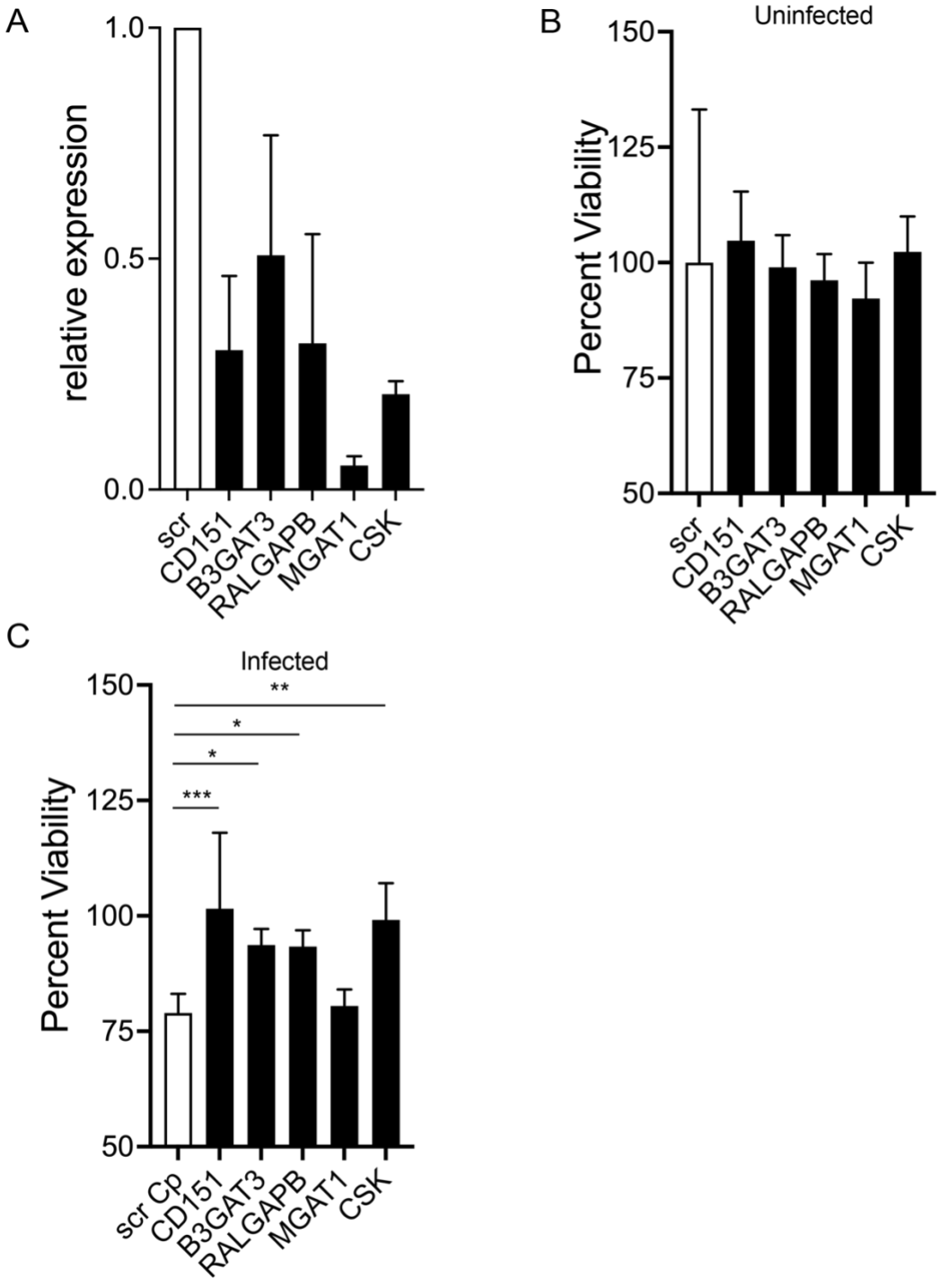

999

1000

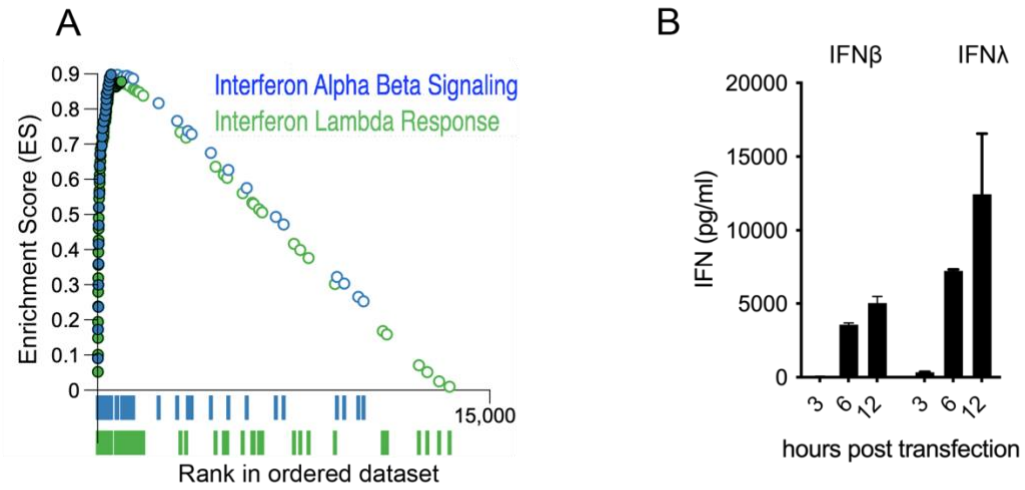

1001

A

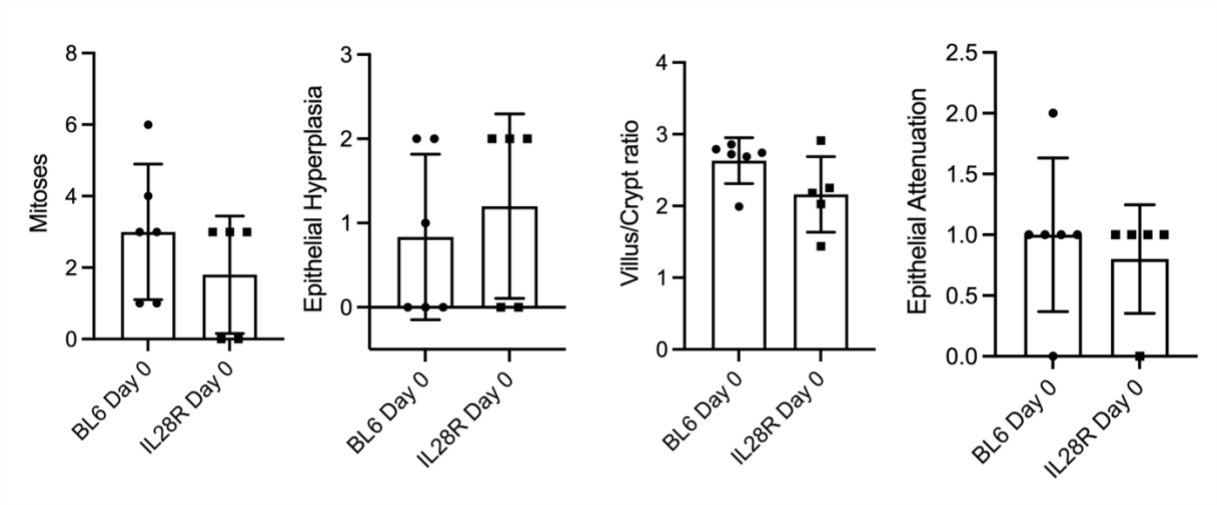

B

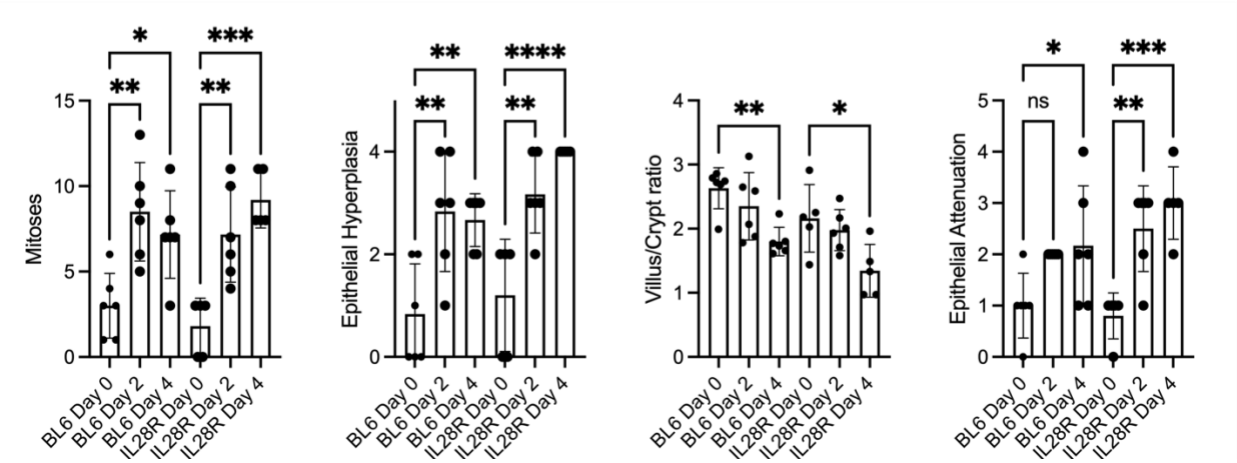

1002

1003

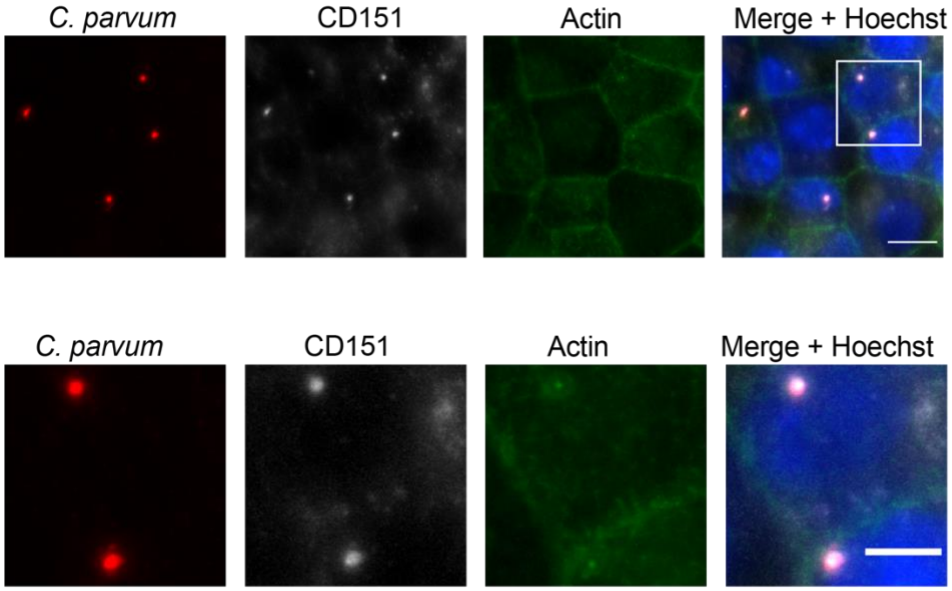

1004

Fig 1. A genome-wide screen reveals genes required for susceptibility to *Cryptosporidium* infection and host cell death

To identify host genes required for *Cryptosporidium* infection we performed a genome-wide knockout screen.

(A) HCT-8 cells infected with increasing numbers of *C. parvum* oocysts are killed in a dose-dependent manner. Host cell viability was assessed by Trypan Blue exclusion. R^2=0.7522

(B) Cas9 activity in different clones of Cas9 expressing HCT-8 cells assessed by flow cytometry normalized to a positive control set to 100 percent.

(C) Schematic of CRISPR screen using *C. parvum* induced host cell death as selection.

(D) Bubble plot of Cas9 expressing Clone K screen showing enrichment of specific genes with each round of selection by *C. parvum* infection. Each bubble represents a human gene and the size of bubbles corresponds to fold change. y-axis is the inverse of the adjusted *p* value.

(E) Bubble plot of concatenation of Clones I and K comparing input to the final selection for 1000-fold coverage. The top 35 genes were colored and grouped based on function. Size of bubbles corresponds to fold change.

Fig 2. *Cryptosporidium* infection induces a type III interferon response in human intestinal epithelial cells

We examined the response to *C. parvum* infection in HCT-8 to determine which specific interferons were induced.

(A) HCT-8 cultures were infected with *C. parvum* oocysts, and RNA was isolated 48 hours post infection from 3 biological replicates and matched uninfected controls. Volcano plot showing differentially expressed genes between uninfected and infected HCT-8 (n=3, biological replicates per group). Genes in red are part of the "REACTOME: Interferon Signaling" signature.

(B) GSEA plot of "REACTOME: Interferon Signaling" signature identified at 48 hours post infection. Closed circles represent genes that make up the core enrichment of the signature. Net enrichment score=3.04, *p* value <0.0001

(C) 96 wells HCT-8 cultures were infected with 25,000 *C. parvum* oocysts for 12-72 hours. Transcript abundance of three representative interferons stimulated genes (ISGs) measured by qPCR is shown over a time course of *C. parvum* infection (n=3)

(D) Immunoblot showing presence of phospho STAT1 and total STAT1 in uninfected cultures and following *C. parvum* infection. Treatment with IFNλ is used as a control for induction of phosphoSTAT1. One representative of 2 biological replicates is shown.

(E) Samples as in (C). Induction of type I (IFNβ) and type III interferon (IFNλ) transcripts as assessed by qPCR. Note peak of *IFNL1*: 35-fold, *IFNL2/3*:1200-fold at 48 hours while peak *IFNB*: 4-fold at 72 hours. *n*=3

(F) Protein levels of type I and type III interferons as assessed by ELISA. Samples as in (C, E) At 48 and 72 hours post infection, the difference between IFNβ and IFNλ was

1046 highly significant. Two-way ANOVA with Dunnett's multiple comparisons **** p <0.0001.

1047 n=3

1048 (G) Relative abundance of *C. parvum* ribosomal RNA transcripts normalized to host

1049 *GAPDH*. n=3

1050

Fig 3. IFN-lambda production requires live infection and is initiated by infected cells

We examined the requirements and kinetics of initiation of the type III interferon response to *C. parvum*.

(A) 24 well HCT-8 cultures were infected with 200,000 *C. parvum* live or heat killed oocysts and protein levels of IFNλ were assessed by ELISA. At 48 and 72 hours post infection the difference between live and heat killed was highly significant. Two-way ANOVA with Šídák's multiple comparisons test **** $p < 0.0001$. $n=3$

(B) Immunoblot comparing induction of STAT1 phosphorylation by infection with live versus heat killed parasites. Phospho STAT1 is only detected in live infection. One representative example of two biological replicates is shown.

(C) Following treatment with nitazoxanide (NTZ), infection is reduced 35-fold as assessed by relative abundance of *C. parvum* ribosomal RNA transcripts normalized to host *GAPDH*. $n=3$

(D) Protein levels of IFNλ in HCT-8 infected with *C. parvum* compared to cultures stimulated with 10μg/mL lipofected Poly(I:C), both in the presence or absence of nitazoxanide. A decrease in IFNλ protein is observed only when NTZ is used in infection. One-way ANOVA with Šídák's multiple comparisons test * $p < 0.05$. $n=3$

(E) Schematic of the 12-hour intracellular cycle of *C. parvum* and outline of a sequencing experiment to examine transcriptional differences between bystanders and infected cells from the same culture.

(F) Immunofluorescence of HCT-8 infected with *Cp* Neon (green) at 10 hours post infection. Hoechst in blue. Scale bar 10μm

(G) Flow cytometry dot plot of infected cells showing green fluorescence and side scatter. Three biological replicates were sorted for Neon positive to Neon negative comparison.

(H) Volcano plot showing differentially expressed genes between Neon negative (bystander) and Neon positive (infected) HCT-8 at 10 hours post infection. Genes in red are ISGs as identified by Interferome DB.

Fig 4. The type III Interferon response is host protective and epithelial cell intrinsic

We used a mouse model of infection to examine the role of type III interferon in *Cryptosporidium* infection *in vivo*. All mice were infected with mouse adapted *C. parvum*.

(A) C57/BL6 (BL6) mice were infected with 50,000 *C. parvum* oocysts and relative abundance of IFNλ transcript is shown for ileal biopsies of infected mice, 4 mice per day, *n*=2

(B) BL6 mice were infected with 50,000 *C. parvum* oocysts and secreted IFNλ protein from ileal biopsies was assessed by ELISA, 2 mice per day, *n*=2

(C) Fecal luminescence measured every two days in BL6 wild type mice, mice lacking the type I IFN receptor $Ifnar^{-/-}$, and mice lacking the type III interferon receptor $Il28ra^{-/-}$ following infection with 50,000 *C. parvum*. A reduction of 3-fold was observed in Ifnar and an increase of 2.7-fold was observed with Il28ra. 4 mice per group. Data shown is representative of 3 biological replicates. (Ifnar: -2.8, -2.9-fold, Il28ra: 2.3, 2.7-fold) n=3

(D) C57/BL6 mice were treated with anti-Ifnλ2/3 antibody or an isotype control daily via intraperitoneal (i.p.) injection and infected. Fecal luminescence was measured every two days. Representative of two biological replicates. An increase of 2-fold was observed in each replicate. *n*=2

(E) $Ifng^{-/-}$ mice were injected i.p. with indicated doses of Ifnλ2 daily for days 0-3 of infection. Mice were infected with 20,000 *C. parvum* oocysts. The total area under the curve of fecal luminescence for the 3-day infection is shown. 2 mice per dose.

Representative of 2 biological replicates (0.1µg: 4.3 and 5.9-fold; 0.5µg: 7 and 1.3-fold; 1µg: 3.8 and 8.8-fold; 5µg: 7 and 18.6-fold). *n*=2

(F) Ifng$^{-/-}$ mice were injected i.p. with 1µg of Ifnλ2 beginning at day 0 and each day for the duration of the infection. Mice were infected with 20,000 *C. parvum* oocysts. Fecal luminescence measured every two days. A 7.7-fold decrease in shedding occurred upon treatment representative of 2 biological replicates (5-fold decrease) *n*=2

(G) BL6 wild type mice, mice lacking T cells Rag2$^{-/-,}$ and mice lacking NK cells, ILCs, and T cells Rag2/Il2rg$^{-/-}$ were treated with 1µg of Ifnλ2 daily for the days 0-3 of infection. The total area under the curve of fecal luminescence for the 3-day infection is shown. (BL6: 2.4, 1.14, 1.22-fold; Rag2$^{-/-}$ 4.4, 1.8, 16.3-fold; Rag2/Il2rg$^{-/-}$ 2, 3.8, 6.5-fold) Representative of 3 biological replicates. *n*=3

(H) Villin Cre STAT1 flox mice or littermate Cre negative controls were treated with 1µg of Ifnλ2 daily for the days 0-3 of infection. The total area under the curve of fecal luminescence for the 3-day infection is shown. Representative of 2 biological replicates (Cre negative: 4 and 2.2-fold; Cre positive: 0.85 and 1.14-fold) *n*=2

Fig 5. TLR3 dependent recognition of *Cryptosporidium* infection

We sought to identify the pattern recognition receptor that is activated to induce IFNλ production in response to *Cryptosporidium* infection.

(A) ELISA of HCT-8 cultures infected with *C. parvum* or treated with the indicated agonist for 24 hours to assess IFNλ production in response to stimulus against a variety of pattern recognition receptors, *n*=3. IFNλ is induced in response to the following stimuli: infection, Poly(I:C), lipofected Poly(I:C), and ssPolyU RNA

(B) Infection of wild type control mice (B6129) compared to mice lacking MAVS. Fecal luminescence measured every 2 days. Representative of 2 biological replicates (1.18 and 1.04-fold increase) *n*=2

(C) Infection of wild type control mice (C57B6N/J) compared to mice lacking TLR7. Fecal luminescence measured every 2 days. Representative of 3 biological replicates (1.3, 0.70, 2.2-fold increase) *n*=3

(D) Infection of wild type control mice (B6129) compared to mice lacking TLR3. Fecal luminescence measured every 2 days. An increase of 8-fold in oocyst shedding was observed. Representative of 3 biological replicates (8, 12.4, 3.8-fold respectively) *n*=3

(E) IL-18 protein detected from ileal biopsies of infected mice wild type (B6129) compared to $Tlr3^{-/-}$ at day 2 post infection. Standard t-test *** p <0.001. 11 mice per group, *n*=2

(F) IFNλ protein detected from ileal biopsies of infected mice wild type (B6129) compared to $Tlr3^{-/-}$ at day 2 post infection. Standard t-test *** p <0.001. 11 mice per group, *n*=2. Dotted line represents the limit of detection.

Fig 6. Model

Cryptosporidium infection leads to sensing by the endosomal pattern recognition receptor TLR3. Following activation of TLR3, IFNλ transcription is induced. Once IFNλ is secreted, it acts first on the infected cell (1), and then on uninfected bystanders (2) to induce the transcription of hundreds of ISGs. Lysis of the host cell by parasite egress releases intracellular contents, including IFNλ, further amplifying the type III interferon response. The protective effects of IFNλ in mice require intact STAT1 signaling in the intestinal epithelial cell lineage. One proposed mechanism of action for IFNλ is to block invasion of the parasite.

S1 Fig. Impact of siRNA knockdown of screening hits on host cell survival upon *C. parvum* infection.

We used siRNA treatment to knockdown transcripts of genes identified in our screen and assessed host cell viability following infection.

(A) Relative expression of genes targeted for knockdown normalized to the scrambled (scr) siRNA control. *n*=2

(B) Knockdown of top candidates does not affect host cell viability in the absence of infection. MTT assay normalized to uninfected scrambled (scr) siRNA control. *n*=2

(C) Knockdown of candidates leads to an increase in host cell viability during *C. parvum* infection. MTT assay normalized to uninfected scrambled (scr) siRNA control. *n*=2

S2 Fig. Type I and type III interferons in HCT-8

(A) GSEA plot showing Interferon Alpha Beta Signaling and Interferon Lambda Response signatures identified at 48 hours post infection. Closed circles represent genes that make up the core enrichment of the signature. Note that many of the genes overlap. Alpha Beta: Net enrichment score=2.9, p-value <0.0001, Lambda: Net enrichment score=3.04, *p* value <0.0001

(B) Protein levels of IFNβ and IFNλ following lipofection with 10μg/mL Poly(I:C) as measured by ELISA. Note the maximal production of IFNβ is 27-fold higher than that observed during *C. parvum* infection

S3 Fig. BL6 and IL28Ra KO mice exhibit similar baseline and post-infection intestinal pathology scores

(A) Histology scoring from uninfected BL6 wild type mice and mice lacking the type III interferon receptor Il28ra$^{-/-}$. No differences were observed.

(B) Histology scoring from BL6 wild type mice and mice lacking the type III interferon receptor Il28ra$^{-/-}$ infected with 50,000 *C. parvum* and uninfected controls. One-way ANOVA with Šídák's multiple comparisons test * p <0.05 ** p <0.01 *** p <0.001 **** p <0.0001. Differences between uninfected Il28ra$^{-/-}$ mice compared to infection tended to be more statistically significant than those observed between uninfected and infected BL6 mice.

S4 Fig. CD151 localizes to the *Cryptosporidium* invasion site

1187 Immunofluorescence of HCT-8 infected with *C. parvum* at 1 hour post infection. *C.*
1188 *parvum* (red), CD151 (gray), actin (green) Hoechst label nuclei. Scale bar 10μm in top
1189 panel, scale bar 5μm in bottom panel

1190

1191 **S1 Table:** List of primers

1192

1193 **S2 Table:** siRNA sequences

1194

1195 **S3 Table:** CRISPR screening data. Summary read count file used for analysis. Summary
1196 of MAGeCK analysis. GSEA for screening data

1197

1198 **S4 Table:** Differential gene expression and GSEA for RNAseq at 48 hours post infection

1199

1200 **S5 Table:** Differential gene expression and GSEA for RNAseq at 10 hours post infection

1201